INFORMATION TO USERS

This manuscript has been reproduced from the microfilm master. UMI films the text directly from the original or copy submitted. Thus, some thesis and dissertation copies are in typewriter face, while others may be from any type of computer printer.

The quality of this reproduction is dependent upon the quality of the copy submitted. Broken or indistinct print, colored or poor quality illustrations and photographs, print bleedthrough, substandard margins, and improper alignment can adversely affect reproduction.

In the unlikely event that the author did not send UMI a complete manuscript and there are missing pages, these will be noted. Also, if unauthorized copyright material had to be removed, a note will indicate the deletion.

Oversize materials (e.g., maps, drawings, charts) are reproduced by sectioning the original, beginning at the upper left-hand corner and continuing from left to right in equal sections with small overlaps.

ProQuest Information and Learning
300 North Zeeb Road, Ann Arbor, MI 48106-1346 USA
800-521-0600

Université d'Ottawa · University of Ottawa

GROUND ICE INVESTIGATION IN THE FAR NORTHWEST OF CANADA

By

Denis Lacelle, B.A. (Honours)

A thesis submitted to the School of Graduate Studies and Research
in partial fulfillment of the Master of Science degree

University of Ottawa / Université d'Ottawa
Department of Geography / Département de Géographie

ABSTRACT

Ground ice formation in the Far Northwest of Canada was investigated using stable isotopes ($\delta^{18}O$ and δD) and ^{14}C dating. These have proven to be valuable tools when inferring the origin of ground ice bodies. The major findings are:

1) During the Late Pleistocene, massive tabular ground ice bodies formed extensively in the Willow River area, Richardson Mountains. These ice bodies are currently exposed in the headwalls of retrogressive thaw slumps as a result of climate warming. Two units were recognized on the basis of ice structure: a debris-rich ice overlain by a diamicton. The debris-rich ice, characterized by low $\delta^{18}O$ values (–30‰ to –27‰), is believed to have formed by *in situ* freezing of subglacial meltwater derived from the Laurentide ice sheet. The meltwater flowed through water-saturated till between relict and aggrading permafrost. A decrease in subglacial meltwater flow from the ice sheet and a decrease in enthalpy transfer from the meltwater caused the freezing of the meltwater within the proglacial water-saturated till. The ice in the diamicton is characterized by relatively high $\delta^{18}O$ values (–26‰ to –20‰) and formed from the freezing of isotopically enriched Holocene waters.

2) In the northern Yukon, a $\delta^{18}O$ analysis of surface and subsurface ice was undertaken. The results indicate that the $\delta^{18}O$ composition of the various ice types is dependent upon a number of factors, such as surface air temperature, relative humidity and freezing rates. Holocene age waters are characterized by $\delta^{18}O$ values > –27‰, while Pleistocene age waters have $\delta^{18}O$ values <–27‰, indicating colder air temperature at the time of precipitation. The effect of evaporation on the isotopic composition of water was best observed on open surfaces where enrichment in the order of 5 – 11‰ in ^{18}O was measured.

ACKNOWLEDGMENTS

I most warmly thank my supervisors, B. Lauriol and I.D. Clark for their support, guidance and encouragements. I am grateful to J. Murton, C. Zdanowicz, J. Veillette, J. Bjornson, and to my committee members, A.G. Lewkowicz and D. Fisher for interesting discussion on the topic. Also, this project could not have been accomplished without the valuable field assistance provided by J. Bjornson, D. Benoit, F. Elanik, D. Charlie, D. Frost and H. Charlie during the 2000 and 2001 field seasons, and a special thanks goes out to the Aklavik and Old Crow communities.

My thanks goes to the staff of the G.G. Hatch laboratory, P. Middlestead, G. St-Jean, and W. Abdy.

A special thanks goes to the "basement brigade" whose humor and company helped make my life as a graduate student very enjoyable. And to my friends across the world, thanks!!

This project was supported by NSERC grants to B. Lauriol and I.D. Clark, Northern Scientific Training Program (NSTP), Polar Continental Shelf Program, Inuvik Research Center (Aurora College) and Yukon Heritage College.

Table of Contents

CHAPTER 1 ..... **1**

SUMMARY **2**

1.1 PERMAFROST AND GROUND ICE TYPES **3**
Massive Ground Ice 3
Buried Ice 5
Intrasedimental Ice 6
Cave Ice 8

1.2 CRYOSTRATIGRAPHY **9**

1.3 STABLE ISOTOPES OF WATER **10**
Fractionation and the meteoric water line 11
Stable isotopes of water (ice) in permafrost 13
Stable isotopes in cave ice 14

1.4 REGIONAL SETTING AND PURPOSE OF STUDY **15**
Objectives 15

1.5 GLACIAL HISTORY, PALEOCLIMATIC RECONSTRUCTION **17**

CHAPTER 2 ..... **19**

SUMMARY **20**

2.1 INTRODUCTION **21**
Scope of study 21

2.2 STRATIGRAPHIC SETTING **23**

2.3 DIAGNOSTIC CRITERIA **24**

2.4 REGIONAL SETTING **26**
Climate 26
Permafrost 27

2.5 METHODOLOGY **30**
Stable Isotope Analyses 30
Gravimetric and Volumetric Water (Ice) Content 31

2.6 RETROGRESSIVE THAW SLUMPS **32**
Cryostratigraphy of exposed headwalls within thaw slumps 32
Unit 1: Debris-rich ice 35
Unit 2: Diamicton 37

2.7 RESULTS **39**
Thaw Slumps 00-2A and 00-2B 40
Thaw Slump 00-4 40

2.8 ORIGIN OF DEBRIS-RICH ICE **43**
Background 43
Origin of ice from $\delta D - \delta^{18}O$ systematic 44
Possible explanation for the formation of the debris-rich ice 49
Hypothesis of formation of debris-rich ice 52

2.9 ORIGIN OF THE DIAMICTON ICE **54**

2.10 SYNTHESIS **57**

CHAPTER 3 ..... **58**

SUMMARY **59**

3.1 INTRODUCTION **60**

3.2 REGIONAL SETTING **61**
Climate 61

3.3 METHODOLOGY **64**
Analytical procedure 64

3.4 RESULTS **65**
$\delta^{18}O$ signature of modern precipitation 65
$\delta^{18}O$ signature of thermokarst lakes 68
$\delta^{18}O$ signature of active layer ice 71
$\delta^{18}O$ signature of ice wedge ice 75
$\delta^{18}O$ variations from a core retrieved from a peat plateau 80
$\delta^{18}O$ signature of Pleistocene segregated ice 82

3.5 DISCUSSION **86**

3.6 FUTURE RESEARCH **89**

REFERENCES **90**

List of Figures

Figure 1.1: A general classification of massive ground ice types. 4
Figure 1.2: A diagram showing the evolution of $^{18}O/^{16}O$ during rainout. 12
Figure 1.3: Location map showing the study areas in the western Canadian Arctic... 16
Figure 2.1: Location map of study sites in the Richardson Mountains, Northwest Territories. 28
Figure 2.2: A) Normal monthly climate data recorded at Inuvik from 1961-1990. 29
B) 5-year running air surface temperature trend recorded from Inuvik compared to mean annual air temperature. 29
Figure 2.3: View of the diamicton (unit 2) and of debris-rich ice (unit 1) exposed in retrogressive thaw slumps. 33
Figure 2.4: A) Visible slump scar located above the headwall of thaw slump 00-2A B) Oblique view and C) Topographic profile of a retrogressive thaw slump in the Richardson Mountains, NWT. 34
Figure 2.5: Volumetric water (ice) content and grain size profiles of thaw slump 00-2B and 00-4. 36
Figure 2.6: Tracing of thin sections from pure ice nodules found in the debris-rich ice. 37
Figure 2.7: Co-isotope diagram showing the isotopic composition of Laurentide ice recorded in Barnes Ice Cap 39
Figure 2.8: A) $\delta^{18}O$ profile from thaw slump 00-2A. B) $\delta^{18}O$ profile from thaw slump 00-2B. C) $\delta^{18}O$ profile from thaw slump 00-4. 42
Figure 2.9: Co-isotope diagram showing the distribution of the ice in the diamicton and the debris-rich ice in all three thaw slumps studied in the Richardson Mountain. ..45
Figure 2.10: Co-isotope diagram showing the distribution of the debris-rich ice with respect to the Wisconsin ice recorded in the Barnes Ice Cap. 45
Figure 2.11: A) Co-isotope diagram showing the distribution of the debris-rich ice in thaw slump 00-2B and 00-4 with respect to the Global Meteoric Water Line. B) Simulation of isotopic evolution of water issued from the Laurentide ice sheet during freezing using a Rayleigh-like distillation. 47
Figure 2.12: Rayleigh-like distillation of a water reservoir as it freezes to completion under (a) open system conditions represented by the δ-open curvve and (b) under closed system conditions represented by the δ-closed curve. 48
Figure 2.13: Schematic representation of the development of tabular ground ice through aggrading permafrost in the Richardson Mountains. 53
Figure 2.14: Conceptual model simulating the vertical transport of $\delta^{18}O$ in a diffusion-dominated system 56
Figure 3.1: Location map of study area in the Northern Yukon. 62
Figure 3.2: A) Normal monthly climate data recorded at Old Crow from 1961-1990. B) 5-years running average air surface temperature trend from Old Crow compared to the mean annual air surface temperature. 63
Figure 3.3: $\delta^{18}O$ vs δD diagram of precipitation collected at Inuvik (1988-1989) and at Mayo (1985-1989) 67
Figure 3.4: A) Enrichment of ^{18}O and D in water during evaporation. B) Isotopic enrichment in evaporating water and the effect of humidity. C) The effect of humidity in evaporating thermokarst lakes in the Old Crow area compared to the calculated evaporation curve in the Old Crow Basin 70

Figure 3.5: Location map showing sampling points of active layer ice in the Bluefish Basin. 72
Figure 3.6: $\delta^{18}O$-δD diagram of active layer ice extracted from drained thermokarstic lakes in the Bluefish Basin compared to the theoretical evaporation curve measured for the area. 73
Figure 3.7: Photograph showing drained thermokarst lakes and lack of vegetation on these surfaces. 74
Figure 3.8: Histogram of $\delta^{18}O$ values of ice wedges located in the Richardson Mountains, from Chiiji'Bluff and from the Rampart of the Porcupine in the Bluefish Basin. 75
Figure 3.9: $\delta^{18}O$ composition of an anti-syngenetic ice wedge located at site 00-3 in the Richardson Mountains. 77
Figure 3.10: Schematic diagram showing the downward growth of anti-syngenetic ice wedge. 77
Figure 3.11: A) Simulation of the isotopic composition of water during melting of a snowpack. B) Co-isotope diagram of three ice wedges located in the western Canadian Arctic compared to the GMWL. 79
Figure 3.12: A) $\delta^{18}O$ profile of porewaters extracted from core BF-1. B) δD– $\delta^{18}O$ diagram of porewaters extracted from BF-1 compared to the GMWL. 81
Figure 3.13: $\delta^{18}O$ - δD diagram showing the possible evolution of water from ice samples collected from the Barnes ice cap (Zdanowicz et al. 2002), glacial meltwater from the Laurentide ice sheet (this study), and segregated ice within the glaciolacustrine sediments of lake Old Crow (this study). 85
Figure 3.14: Synthesis of the range and kinetic effect on $\delta^{18}O$ and δD in meteoric, surface and subsurface ice in the western Canadian Arctic. 88

List of Tables

Table 2.1: Radiocarbon dates obtained from retrogressive thaw slumps in the western Canadian Arctic. 38
Table 2.2: CO_2 pressure, concentration, and $\delta^{13}C$ values obtained by dry extraction of CO_2 from ice nodules found in the debris-rich ice at site 00-5. 51
Table 3.1: Weighted mean $\delta^{18}O$ values and *d* values for Inuvik and Mayo. 67
Table 3.2: $\delta^{18}O$ and δD variations of active layer ice in the Bluefish Basin. 73
Table 3.3: $\delta^{18}O$ and δD values of segregated ice found within the glaciolacustrine sediment deposited by glacial lake Old Crow 84

CHAPTER 1

GENERAL INTRODUCTION

SUMMARY

This chapter describes the origins of various types of ice found in frozen sediments in the western Canadian Arctic. It also introduces the aspects of geocryology used in this study, primarily the analysis of the stable isotopes of water ($\delta^{18}O$ and δD) and cryostratigraphy. Finally, a description of the paleoclimate and glacial history of the region is presented.

1.1 PERMAFROST AND GROUND ICE TYPES

Permafrost is a subsurface phenomena related to ground temperatures being at, or below 0°C for at least two years (ACGR 1988) and gives rise to unique terrain conditions and landforms. Permafrost underlies approximately half of Canada and contains variable amounts of ground ice.

Ground ice is a general term used to designate all types of ice found in permafrost. Ground ice occurs in pores, cavities, voids, and other openings in soil or rock and includes massive ground ice (ACGR 1988). Although the traditional usage of the term has excluded buried glacier ice (Mackay 1972), a recent trend is to consider buried ice (i.e. glacier, lake, river, or snow bank ice) as one type of ground ice. Thus any type of ice found within frozen sediments can be classified as 1) "*buried ice*", which includes surface ice and glacier ice, 2) "*intrasedimental ice*", which includes ice wedges, injection ice, segregated ice, and aggradation ice, or 3) "*cave ice*" which includes ice plugs, wall ice and floor ice (Figure 1.1).

Massive Ground Ice

Massive ground ice is defined on the basis of ice content and ranges in volume from tens of cubic centimeters to thousand of cubic meters. Massive ice bodies typically have an ice content averaging 250% on an ice-to-dry soil weight basis for thickness of several meters (ACGR 1988). When the gravimetric ice content is less than 250%, it is termed "icy sediment".

Massive ground ice is widespread in the western Canadian Arctic. Tabular massive ground ice has been observed in the interior Yukon (French and Pollard 1986), along the

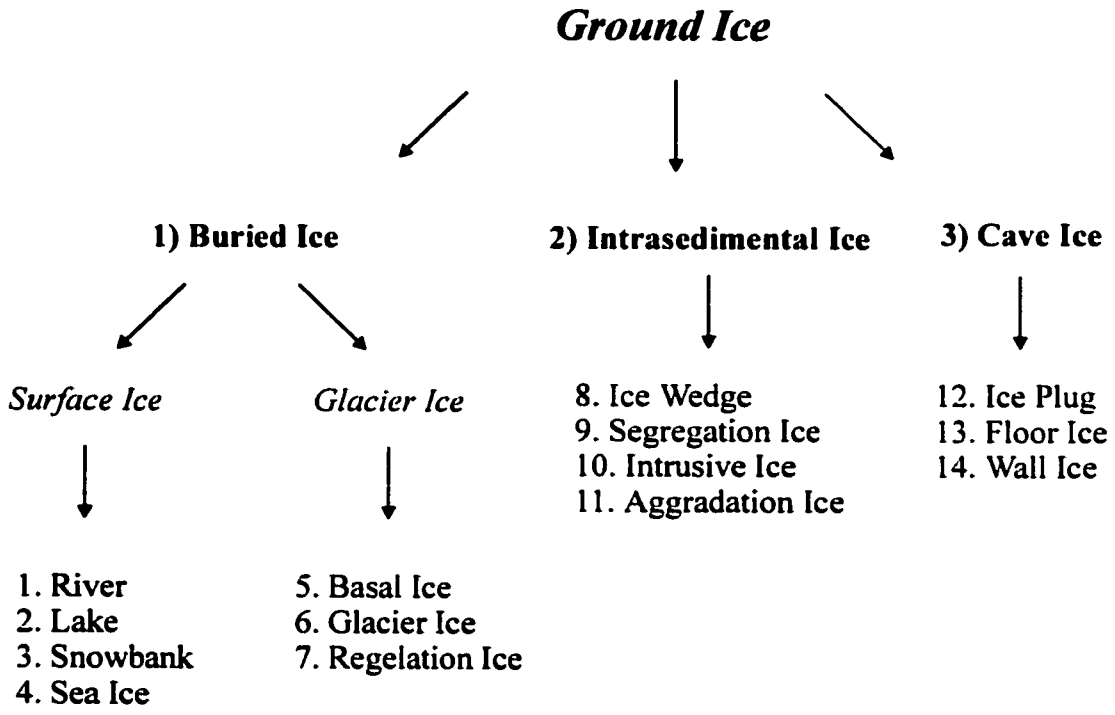

Figure 1.1: A general classification of massive ground ice types (modified from French 1996).

Yukon Coastal Plain (Harry et al. 1988; Pollard and Dallimore 1988), and throughout the Mackenzie Delta (Mackay 1966; Dallimore and Wolfe 1988; Rampton 1988; Fujino et al. 1988). Massive ground ice takes several forms: ice lenses, pingo ice, ice wedges, and tabular massive ground ice. The development of pingos and ice wedges are fairly well understood. However, the origin and processes that form tabular massive ground ice are still not well understood. The two main theories usually suggested for the origin of massive ground ice bodies are: (1) *buried glacier ice* (i.e. remnants of the Laurentide ice sheet), or (2) *intrasedimental ice* (segregation/intrusive origin). Other theories that have been advanced to explain the formation of massive ice bodies include: buried lake, river, sea ice, or metamorphosed snow bank ice (French and Pollard 1986).

Buried Ice

A buried glacier ice origin has been proposed for several thick, tabular ice bodies observed in the glaciated permafrost regions of western Canadian Arctic (Lorrain and Demeur 1985; French and Harry 1990; St-Onge and McMartin 1995, Worsley 1999) and northwestern Siberia (Astakhov 1986; Kaplanskaya and Tarnogradski 1986; Karpov 1986). Most of the buried massive tabular ground ice bodies in the western Canadian Arctic and in northwestern Siberia occur near the limits of known glaciations. They are most probably the result of incomplete deglaciation and are protected from further thaw by a cover of glacigenic material. In the continuous permafrost environments, the debris overburden may exceed the active layer thickness, preventing the glacier ice from further thaw.

In the unglaciated Klondike area, French and Pollard (1986) suggest that a large ice body found within frozen sediments was a buried snow bank, which had been metamorphosed into massive ice.

Intrasedimental Ice

Many types of intrasedimental ice are documented. Ice wedges are the easiest to recognize, whereas segregated ice, injection ice, and aggradational ice are other main types of intrasedimental ice.

Ice wedges are one of the most characteristic features in permafrost terrain. Their formation requires the presence of permafrost. They have been extensively studied by J.R. Mackay (1972; 1986; 1990a; 2000) in the Mackenzie Delta region for over three decades. Ice wedges have a climatic or paleo-climatic significance, since they develop only in areas where the mean annual air temperature is below -6°C (Kasper and Allard 2001). Ice wedges commonly join to form ice wedge polygons, which are easily observable in lowland setting. Mackay (1990a) proposed a classification system for ice wedges based on their growth direction. Epigenetic ice wedges grow where there is negligible addition/loss of material at the ground surface during ice wedge growth, and are, consequently, younger than the enclosing material. Syngenetic ice wedges develop where there is accumulation of material to the ground surface during ice wedge growth and tend to have a chevron growth pattern (Lewkowicz 1994). Anti-syngenetic ice wedges, as their name implies, grow downwards on hillslopes during the removal of surface material.

Segregated ice is a general term for soil with high ice content (French 1996, p.87). Segregated ice lenses vary in thickness from layers a few centimeters thick to massive tabular ice bodies up to several meters thick (ACGR 1988). Typically, ice lenses are best developed in fine-grained sediments where the water content is high and cryosuction can be easily maintained, thereby continuously supplying the growing ice lenses. Such sediments are often termed "frost-susceptible". Pore ice, by contrast, commonly develops in coarser-grained sediments (i.e. sand, gravel) where it is harder for cryosuction to be maintained in the correspondingly larger soil interstices. Palsas, which are large masses of segregated ice formed within peat or mineral soil, are regarded as one of the few surface indicators of discontinuous permafrost (Pollard and French 1984). Palsas must not be confused with seasonal frost mounds. The latter form by water injection and are characterized by a core of pure ice, with ice crystals aligned vertically reflecting the direction of the freezing plane (Pollard and French 1984; 1985), while palsas form by ice segregation.

It is often difficult to differentiate between massive tabular segregated ice and buried glacier ice, and this question will be examined in chapter 2.

Intrusive ice is formed by the intrusion of water, usually under pressure, into permafrost from a proximal source causing the ground above it to uplift when it freezes (Mackay 1972). Sill and pingo ice are the two types of intrusive ice usually identified. Sill ice grows when water is confined and freezes along the base of the active layer and parallel to the permafrost table. Open-system pingos, which are ice-cored hills that are uplifted by the intrusion of water under pressure, are geomorphic features typical of such ice growth. Other surface features of permafrost formed by similar processes to open-

system pingos are seasonal frost mounds, however, their growth is limited within the active layer (French 1996).

Aggradational ice is unique to permafrost terrain. It forms when the upper permafrost surface gradually rises over a period of years, either by the addition of sediment to the surface (e.g. alluvial, eolian, or peat growth), or by a decrease in the thickness of the active layer (Mackay 1972). In doing so, segregated ice lenses become incorporated at the top of the new permafrost. In many areas, thick ground ice layers may develop in the top of permafrost, mostly in fine-grained soils (Cheng 1983) due to repeated aggradation and annual accumulation of water.

Cave Ice

Massive ice formation in karst cave passages in alpine and permafrost regions are not uncommon (Schroeder 1977; Lauriol and Clark 1993). Massive ice blockages in caves are formed by gradual accumulation of floor ice and accretion of ice growing down from the cave roof resulting in the development of an ice plug on a face contiguous with floor ice below and frost on the cave roof.

1.2 CRYOSTRATIGRAPHY

Cryostratigraphy is the study of the shape and distribution of ground ice within perennially frozen ground. Murton (1993) established a simple and comprehensive classification system of cryostructure and cryofacies. Five categories of cryostructures were defined that are visible to the naked eye and are similar to sedimentary structures. Ice lenses can be described by their shape as planar, wavy, or curved, and either layered or lenticular. Murton (1993) also defined five categories of cryofacies based on their volumetric ice content:

(1) Pure ice (100%)

(2) Sediment-poor ice (≥ 90% volumetric ice content)

(3) Sediment-rich ice (50 - <90% ice)

(4) Icy sediment (excess ice - <50% ice)

(5) Ice-poor sediment (no excess ice).

The first four are thaw sensitive and are prone to thermokarst, while the fifth is thaw-stable.

1.3 STABLE ISOTOPES OF WATER

The chemical nature of an element is defined by its atomic number and electron configuration. For example, heavy water, $^{2}H_{2}{}^{16}O$, has a mass of 20 compared to normal water, $^{1}H_{2}{}^{16}O$, which has a mass of 18. Variation in the number of neutrons of an element lead to a variety of isotopes (e.g. ^{18}O, ^{17}O, ^{16}O) and isotopic processes, called partitioning.

The most common isotopes of water are ^{16}O (99.63%) and ^{1}H (99.98%). Four other isotopes (^{18}O, ^{17}O, ^{3}H, and D or ^{2}H) exist but are much less abundant, of which ^{18}O, ^{17}O and ^{2}H are stable and ^{3}H radioactive (half-life = 12.43 years). Isotopic concentration or abundance is measured as the ratio of the two most abundant isotopes of a given element (e.g. $^{18}O/^{16}O$ or D/H). Water samples are routinely analysed against Vienna Standard Mean Ocean Water (VSMOW). VSMOW has an $^{18}O/^{16}O$ abundance ratio of 2.0052×10^{-3} and $^{2}H/^{1}H$ a ratio of 1.5575×10^{-4} (Clark and Fritz 1997). Changes in the abundances of ^{18}O and D with respect to these standards are expressed as $\delta^{18}O$ and δD, where:

$$[1] \qquad \delta = (R_{sample} - R_{standard} \times 1000) / R_{standard}$$

where: R is the isotope ratio of $^{18}O/^{16}O$ or D/H.

The changes in abundance are referred to as delta-values expressed as parts per thousand differences between the sample and the reference. A δ-‰ value that is –10‰ signifies that the sample has 10‰ less ^{18}O than the reference, or is 10‰ depleted. The most important control on the isotopic composition of water is surface air temperature (Craig 1961).

Fractionation and the meteoric water line

If a body of water is left to evaporate, the lighter isotopes (^{16}O and ^{1}H) of water will preferentially evaporate, thereby enriching the remaining water in the heavier isotopes (^{18}O and D). Upon condensation, the opposite occurs and the heavier isotopes are preferentially removed, thus leaving the residual water vapour depleted. The main reason for fractionation of the three most important isotopic components of water ($H_2{}^{16}O$, $HD^{16}O$, and $H_2{}^{18}O$) is that the water vapour pressure of the heavier component is slightly lower than the light component (Dansgaard 1964). Hence, water vapour is isotopically depleted with respect to source water during evaporation. Global precipitation follows a Rayleigh-type distillation process (Figure 1.2). This means that if water vapour separates from the ocean and travels towards higher latitudes, the first precipitation to form will be enriched in heavier isotopes, and the last to form will be significantly depleted (Craig 1961; Dansgaard 1964).

Dansgaard (1964) established a linear relationship between annual air surface temperature and $\delta^{18}O$.

$$[2] \qquad \delta^{18}O = 0.695T - 13.6‰$$

Where, T is the mean annual air temperature at the ground surface and $\delta^{18}O$ represents the mean annual value at the site. This relationship is due to the fact that precipitation and rainout are driven by decreasing temperature.

Although this relation should not be used directly, it is essential to note that a decrease in surface air temperature is associated with a decrease in $\delta^{18}O$ in precipitation. Providing that no major isotopic changes have occurred by mixing, evaporation or fractionation between the time of precipitation and freezing, $\delta^{18}O$ values should reflect

the temperature or paleo-temperature at the time of precipitation (Dansgaard 1964). Nikolayev and Mikhalev (1995) have used samples from Siberia to correlate $\delta^{18}O$ variations with surface air temperature at the time of formation of ground ice.

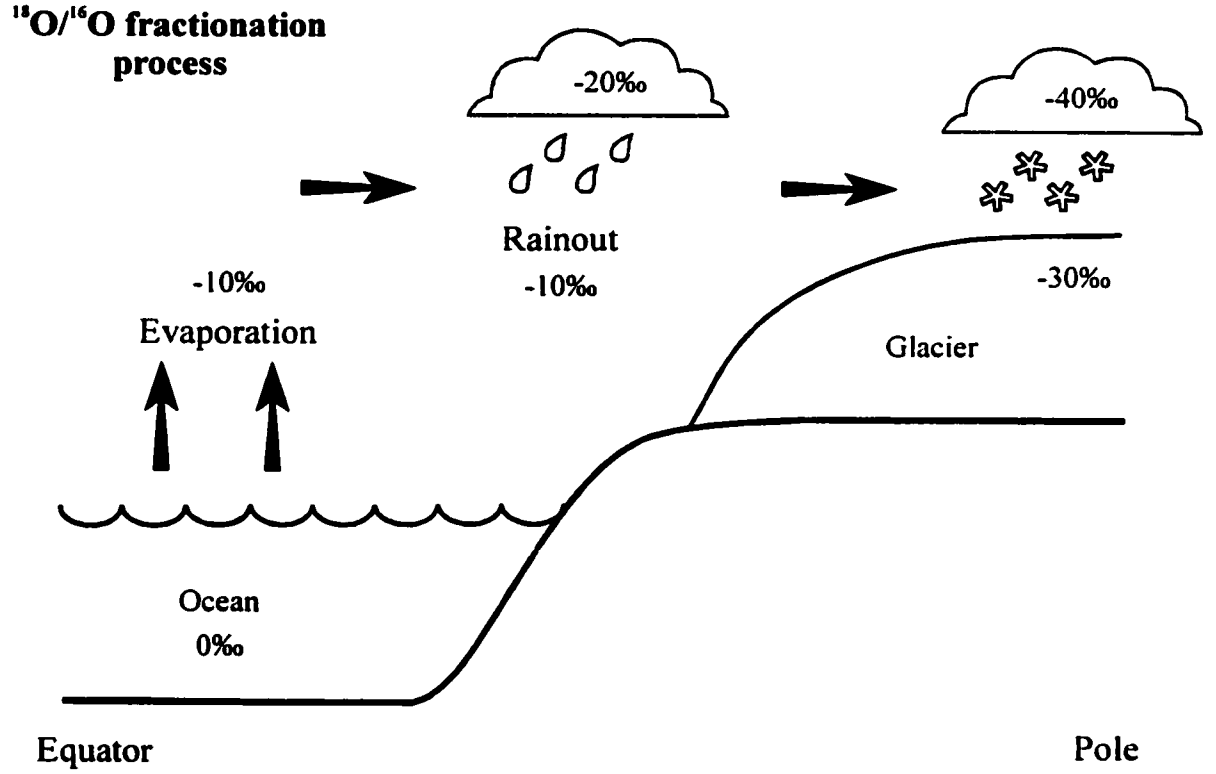

Figure 1.2: A generalized diagram showing the evolution of $^{18}O/^{16}O$ during rainout. If water vapour evaporates from the ocean and travels toward higher latitudes, it is cooled and the vapour becomes progressively depleted in heavy isotopes according to a Rayleigh-type distillation process. This means that precipitation forming at lower latitudes will be enriched in heavier isotopes, and precipitation forming at higher latitudes will be significantly depleted.

The relation between $\delta^{18}O$ and δD in most global precipitation is characterized by the Global Meteoric Water Line (GMWL) and is expressed as:

[3] $\delta D = 8\,\delta^{18}O + 10‰$ (Craig 1961)

Local meteoric water lines (LMWL) have been determined for several stations in Canada. The Canadian meteoric water line is,

[4] $\delta D = 7.75\,\delta^{18}O + 9.83‰$ (Clark and Fritz 1997),

whereas, the meteoric water line for Inuvik is,

[5] $\delta D = 7\,\delta^{18}O - 12.02‰$ (Vardy et al. 1998).

Stable isotopes of water (ice) in permafrost

The isotopic composition of water provides a tool to distinguish between waters of different origins. Also it is an important component of cryostratigraphy, since it is helpful in estimating paleo-climatic conditions during the formation of ground ice, even though it may be derived from precipitation whose $\delta^{18}O$ may vary considerably seasonally and annually. Stable isotope analyses of ground ice may also be useful in the interpretation of permafrost stability and history where the identification of isotopic discontinuities (thaw unconformities), caused by changing climate, may be revealed within the frozen sediments (Michel and Fritz 1982; Michel 1982; Murton and French 1994; Burn 1997).

Isotopic discontinuities revealed within permafrost have been related to long-term temperature changes associated with glacial/non-glacial intervals. In the western Canadian Arctic, Pleistocene sediments have lower $\delta^{18}O$ values ($< -27‰$), than modern

icy sediments (~ –21‰), indicating that temperatures at the time were colder than at present.

Ice originating directly from atmospheric sources (rain, snow) that has been subjected to minimal melting-freezing events gives a slope of ~ 8 in a δD–$\delta^{18}O$ diagram (Craig 1961). For ice with a segregated origin, the slope might be closer to six (Jouzel and Souchez 1982), and ice derived from freezing in a closed system may exhibit a slope closer to five (Souchez and Jouzel 1984). Injection ice (pingo ice) has exhibited a slope of 7.2 (Mackay 1990b). Although the ice is derived from the freezing of groundwater in a closed system, the co-isotope slope lies along the meteoric water line, indicating that the slope may not always be diagnostic of water origin (Mackay 1990b; French and Harry 1990).

Stable isotopes in cave ice

Massive ice formation is karst cave passages in permafrost regions are not uncommon (Lauriol and Clark, 1993). Ice formation in cave is sensitive to seasonal air circulation. The stable isotopes of annual ice from caves are enriched in D and plot above values of the local meteoric water line, which is consistent with formation during summer by condensation and freezing of warm humid air (isotopically enriched vapour) flowing inward along the cave roof. In the winter, reverse circulation of the cave's atmosphere causes vapour in the cold dry air entering the cave to sublimate onto much of the ice mass formed during the summer.

1.4 REGIONAL SETTING AND PURPOSE OF STUDY

The study area is located in the far northwest of Canada (Figure 1.3), mostly in the Richardson Mountains and Northern Yukon (Old Crow – Bluefish Basins). The Richardson Mountains represent the maximum westward limit of the Laurentide ice sheet some time prior to late Wisconsin, while the Old Crow-Bluefish Basin lies in the middle of Beringia, an unglaciated region.

The purpose of the research is to improve our understanding of the formation of massive ground ice bodies in the western Canadian Arctic inferred from $\delta^{18}O$ and δD. This investigation may provide insight into the geological history and potential regional distribution of ground ice.

Massive ground ice occurrences in the western Canadian Arctic are not uncommon but their origin and age are not readily apparent. In this thesis, stable isotopes and ^{14}C dating are used in order to try to elucidate the formation of ground ice. Also a synthesis of the isotopic signature of surface and subsurface ice is provided.

Objectives

A) Richardson Mountains, Northwest Territories:

To determine the mode of formation of tabular ground ice bodies in the Richardson Mountains, a glaciated region.

B) Old Crow-Bluefish Basin, Yukon Territory:

To determine the isotopic signature of surface and subsurface ice in relation to surface air temperature, humidity and freezing rate conditions.

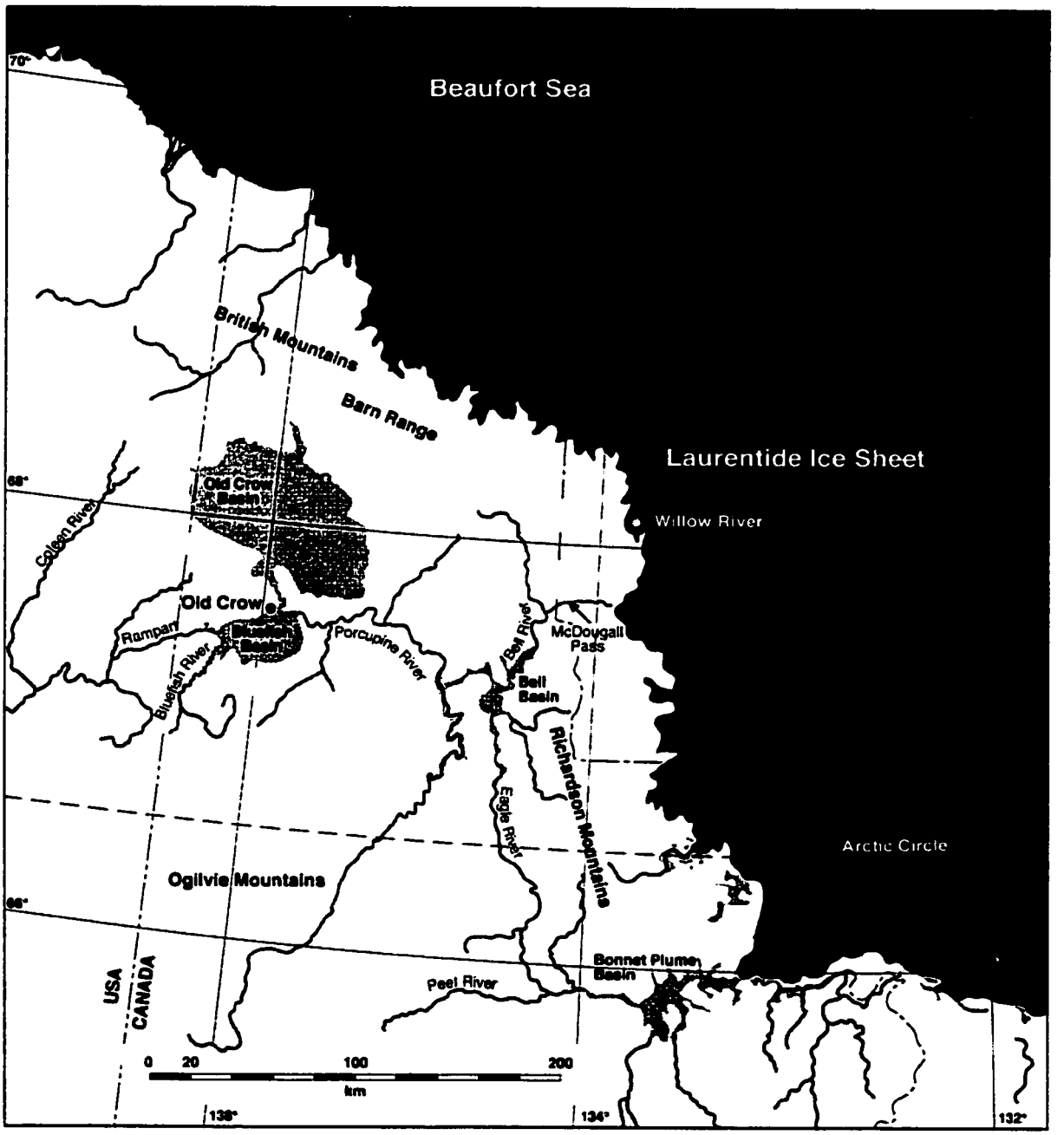

Figure 1.3: Location map showing the study areas in the western Canadian Arctic. Willow River (Richardson Mountains) is located within the maximum glacial extent of the Laurentide ice sheet, while the Bluefish Basin lies in the middle of Beringia.

1.5 GLACIAL HISTORY, PALEOCLIMATIC RECONSTRUCTION

During the last glacial maximum, around 30,000 BP (Duk-Rodkin and Hughes 1992), the Laurentide ice sheet filled the McDougall Pass and Bonnet Plume Depression in the Richardson Mountains, blocking the eastward drainage of the Porcupine and Peel Rivers, thereby causing the inundation of the Old Crow – Bluefish Basins with the formation of glacial lake Old Crow (Lemmen et al. 1994). At about 12,500 BP, a new outlet formed through the Ramparts of the Porcupine, which allowed for the westward drainage of Lake Old Crow to the Yukon River. The ice had retreated east of the northern Mackenzie Delta and Richardson Mountains by 13,000 BP allowing for the development of an extensive proglacial drainage system into the Beaufort Sea (Lemmen et al. 1994). Permafrost was established in the Old Crow – Bluefish Basins by 10,000 BP (Dyke 1996).

Pollen and fossil evidence (Hughes et al. 1981) suggest that the climate was much colder and arid than present from 30,000 BP to 16,000 BP. The climate in the unglaciated Old Crow Basin during this period was strongly influenced by the presence and behavior of the Laurentide ice sheet to the east and from the Cordilleran ice sheet to the south. From 11,000 to 8,000 BP, the climate warmed rapidly and was much warmer and drier than today (Lauriol et al. 2002). Some authors suggest that temperatures were 3°C to 6°C warmer than present day values from around 10,000 to 7,500 BP (Ritchie 1984). Investigations by Burn (1997) showed that the active layer was one and a half times thicker than today around 8,500 BP in the Mackenzie Delta under the effect of climatic improvement and of the coastline being further north. Rampton (1982) suggested a period of important thermokarst activity during this period. From 8,000 BP

to 4,000 BP, the climate was wetter with total annual precipitation 12 cm greater than at present (Ritchie 1984; Lauriol et al. 2002). After 5,000-4,000 BP, the climate remained comparable to present day values with some minor fluctuations (e.g. the Medieval Warm Period and the "Little Ice Age").

During the last 70 years, a warming trend of 0.25°C per decade was recorded at Inuvik's meteorological station, which has resulted in an increase of about 1.25°C in the mean annual air temperature (Environment Canada 2001). This is one of the most dramatic climatic warming trends in the Canadian Arctic. However, this warming trend is not distributed equally by decades. In the last decade, surface air temperatures increased by 0.9°C (Parks Canada 2000).

CHAPTER 2

FORMATION OF TABULAR GROUND ICE BODIES INFERRED FROM ISOTOPIC ANALYSES, RICHARDSON MOUNTAINS, N.W.T.

SUMMARY

The two main theories explaining the formation of tabular ground ice in the western Canadian are (1) *intrasedimental ice* and (2) *buried glacier ice*. Extensive beds of tabular ground ice have been exposed in the headwalls of retrogressive thaw slumps in the Richardson Mountains, N.W.T. Based on their facies, two units have been recognized in the headwalls: (1) a debris-rich ice overlain by (2) a diamicton. Stable isotopes analysis ($\delta^{18}O$ and δD) and ^{14}C dating indicate that the tabular debris-rich bodies are of Pleistocene age. The debris-rich ice bodies are characterized by low $\delta^{18}O$ values (–30‰ to –27‰) and are believed to have formed from subglacial meltwater issuing from the Laurentide ice sheet. The subglacial meltwater flowed through an aquifer and froze *in situ* as a result of aggrading permafrost and decreasing meltwater fluxes which reduced the transfer of heat from the meltwater. The ice in the diamicton is characterized by relatively high $\delta^{18}O$ values (–26‰ to –20‰) and formed from the freezing of isotopically enriched meteoric Holocene waters. Detailed $\delta^{18}O$ profiles measured through the exposed ground ice indicate a diffusion-dominated profile. A conceptual model simulating the vertical transport of $\delta^{18}O$ suggests that the development of such a profile occurred during the early Holocene warm climatic interval and that it was subsequently preserved by aggrading permafrost.

2.1 INTRODUCTION

Natural exposures of massive ground ice and icy sediments have been reported from glaciated permafrost regions of western Canadian Arctic and northwestern Siberia. Massive ground ice bodies can be defined as large tabular bodies of ground ice whose gravimetric ice content exceeds 250% (ACGR 1988), whereas icy sediments contains excess ice and have an ice content below 250% (ACGR 1988). In the western Canadian Arctic, massive ground ice and icy sediments have usually been interpreted has *intrasedimental ice* (Mackay 1966; Mackay 1971; French and Pollard 1986; Dallimore and Wolfe 1988; Harry et al. 1988; Pollard and Dallimore 1988; Rampton 1988*a*; Mackay and Dallimore 1992), whereas in northwestern Siberia, a *buried glacier ice* origin has a greater importance in the Russian literature (Astakhov 1986; Kaplanskaya and Tarnogradski 1986; Karpov 1986).

Distinguishing between both intrasedimental ice and buried glacier ice is fundamental to better understand massive ice genesis and glacier–permafrost interactions at the margin of the ice sheet. However, the proper interpretation of massive ground ice and icy sediments is often subject to debate (French and Harry 1990). It may be difficult to distinguish between both ice types without detailed physical and chemical examination, since their ice facies may appear very similar (Klassen and Shilts 1987) and may also be genetically similar (Mackay 1989).

Scope of study

Most of the previous studies examining massive ground ice and icy sediments in the Mackenzie Delta and northern Yukon focused on natural sections outcropping along

the shores in the receding headwalls of retrogressive thaw slumps (Mackay 1989). According to Lewkowicz (1986), coastal erosion is responsible for the initiation of most of these slumps. This chapter discusses the origin of non-glaciotectonically deformed massive ground ice and icy sediments exposed in the headwalls of retrogressive thaw slumps on the Aklavik plateau, ~100 m above Willow River, in the Richardson Mountains.

The origin of tabular ground ice bodies has been studied from various perspectives, and stratigraphic settings (Rampton 1988; Mackay 1989), crystallographic observations (Pollard Dallimore 1988) and stable isotope analyses (Lorrain and Demeur 1985; Mackay and Dallimore 1992) have been well documented. The objectives of this chapter are to: (1) Characterize the origin of exposed ground ice bodies through detailed $\delta^{18}O$ profiles and (2) Comment on the sub-glacial thermal regime of the northwestern lobe of the Laurentide ice sheet. These objectives will allow for a better comparison between intrasedimental ice and buried glacier ice.

2.2 STRATIGRAPHIC SETTING

In general, the stratigraphic setting for massive tabular segregated ice from the surface downward is as follows: a reworked clayey till; massive ice; sand and gravel commonly inter-layered with ice (Mackay and Dallimore 1992; French 1996). The massive ice in the Tuktoyaktuk Peninsula is usually interpreted to have developed from the freezing of glacial meltwater that flowed under substantial pressure through permeable unfrozen sands. For example, the $\delta^{18}O$ values of about –30‰ are in the same range as those reported for mid to late Wisconsin ice in the Canadian Arctic Islands ice caps (Paterson et al. 1977; Zdanowicz et al. 2002).

Basal glacier ice may contain significant amounts of stratified layers of debris formed by regelation and congelation as a consequence of both pressure-melting conditions and freezing-on at the glacier's sole (Souchez et al. 1988; Hubbard and Sharp 1997; Knight 1997). Regelation ice results from localized melting and refreezing of glacial water generating laminations of clean ice and debris. The thickness of the layers is limited to the size of the larger obstacles and rarely exceeds the centimeter (Hubbard and Sharp 1997). Congelation ice results from the bulk freezing of water at the base of the glacier. Congelation ice also results in lamination of clean ice and debris bands but at a larger scale as water reaching the bed from extra-glacial lakes or streams can import substantial amounts of debris to the bed. Freezing will often result in the expulsion of suspended fine sediment from the water and the formation of clean ice. Metamorphic processes (glaciotectonic deformation) within the ice close to the bed can form non-stratified (dispersed) debris facies of basal glacier ice.

2.3 DIAGNOSTIC CRITERIA

Currently, a number of parameters (e.g. stratigraphic setting, ice crystallography and stable isotopes) can be used to characterize massive tabular ground ice bodies. Mackay (1989) has described several stratigraphic features that may help to distinguish between buried glacier ice and intrasedimental ice. The diagnostic criteria relate mainly to the contact between the ice and the overlying/underlying material. Buried glacier ice must be older than the overlying material; therefore the upper ice-soil contact must represent an erosional or unconformable surface. By contrast, massive segregated ice bodies commonly have a gradational or conformable contact with the overlying material. Rampton (2001) also suggested that, in most areas, a till should underlie buried glacier ice.

Another aspect that helps in the identification of the origin of massive tabular ground ice bodies is stable isotope analysis. In general, an abrupt isotopic discontinuity should exist between buried glacial ice and overlying material because of different water sources. In a massive segregated ice body, there may be a progressive change in the isotopic composition with depth. However, Mackay and Dallimore (1992) observed a linear isotope profile through massive segregated ice and underlying sandy sediment indicating a common water source and downward freezing.

In general, the bulk chemical and isotopic composition of basal glacier ice should reflect that of glacier ice, as there is little interaction with the underlying sediment during thawing and refreezing of meltwater at the glacier's sole. Souchez and de Grotte (1985) have suggested three possible situations that might occur at the basal (ice-bedrock) interface and which could be identified using co-isotopic measurements:

(1) If water melted in the interior of a glacier, or ice sheet, and re-freezes entirely at the sole, a closed system applies and basal ice samples will be aligned along on slope less than 8. This model only applies to the regelation process or to certain instances of marginal refreezing of basal melt. This case was observed at Aktineq glacier on Bylot Island (Souchez et al. 1988) and at Glacier B-7 on Bylot Island (Zdanowicz et al. 1996).

(2) If water of similar isotopic composition is supplemented to subglacial water during refreezing, then the open system model of Souchez and Jouzel (1984) applies, which allows for mixing during refreezing. A freezing slope similar to that resulting from the closed system conditions is produced but with individual ice samples plotting as richer in heavy isotopes than the initial water.

(3) If lighter isotopic water is mixed with the initial water, basal ice samples may be aligned on a slope steeper than the freezing slope, and eventually may be indistinguishable from the slope of glacier ice depending on the input rate to freezing rate coefficient. The freezing slope is similar to the GMWL when the isotopic composition of the input water is significantly different than the initial water, or when the freezing rate follows the input rate.

The δD vs $\delta^{18}O$ relationship allows one to follow the process by which the two heavy component of water behave in different ways. In general, co-isotope slopes greater than seven suggest that the ice originated from atmospheric sources that have been subjected to minimal melting-freezing events or evaporation. Co-isotope slopes less than seven indicate freezing of groundwater in an open system. While co-isotope slopes less than six are thought to have formed from groundwater during freezing in a semi-closed

system, and co-isotope slopes less than five, to have formed from the freezing of groundwater in a closed system.

2.4 REGIONAL SETTING

The Richardson Mountains consist of a complex of folded anticlines with north-south trending ridges, stretching over 300 km from its southern extremity near the Peel River to within 35 km of the Arctic Coast. Relief throughout the range is generally less than 500 m, and the topography is "more similar to that of foothills rather than a major mountain chain" (Bostock 1948). Along the eastern edge of the mountains bordering the Mackenzie Delta, an escarpment 600 m high marks the mountain front of the Aklavik Range. The study area is located within the Willow River's drainage basin (67°55'N ; 135°48'W) (Figure 2.1). A distinct characteristic of the terrain is its non-glacial mountainous relief (> 750 m) including cryoplanation terraces (Lamirande et al. 1999) adjoining a glaciated lowland (< 700 m) covered by a till veneer (Duk-Rodkin and Hughes 1992). Quartzites, sandstones, siltstones and shales of the Jurassic Bug Creek Formation and clastic rocks of the Jurassic/Lower Cretaceous Husky Formation underlie much of the study area (Norris 1984).

Climate

The study area has a subarctic continental climate characterized by cold, dry winters and short summers. Mean July temperature, derived from Inuvik's meteorological station, is 14°C, while the January mean value is –29°C (Figure 2.2 A; Environment Canada 2001). The mean annual temperature ranges from –10°C at Inuvik to –15°C in

the Richardson Mountains (Burns 1974). During the last 20 years, the surface air temperature has increased by 1.7°C, one of the most dramatic climatic warming trends in the Canadian Arctic (Figure 2.2 B)

Precipitation along the eastern slope of the Richardson Mountains amounts to 250 mm/yr, of which 120-130 mm is rain and the remainder snow (Figure 2.2 A; Environment Canada 2001).

Permafrost

The study area is located within the continuous permafrost zone (Brown 1978). Permafrost thickness reaches 100 m at Inuvik and is estimated to be in excess of 300 m in the Richardson Mountains (Judge 1973). Thawed layer thickness was measured at 0.6 m during early July 2000 in the Willow River area, but the active layer probably varies from 0.5 m in fine clay sediments to 4 m in some coarse sediments (Catto 1986). Any thawing of the permafrost, either through climatic change, fluvial erosion, or removal of vegetation, creates the potential for mass movement. Numerous retrogressive thaw slumps are present throughout the vicinity of Willow River, which is indicative of a widespread distribution of tabular ground ice bodies.

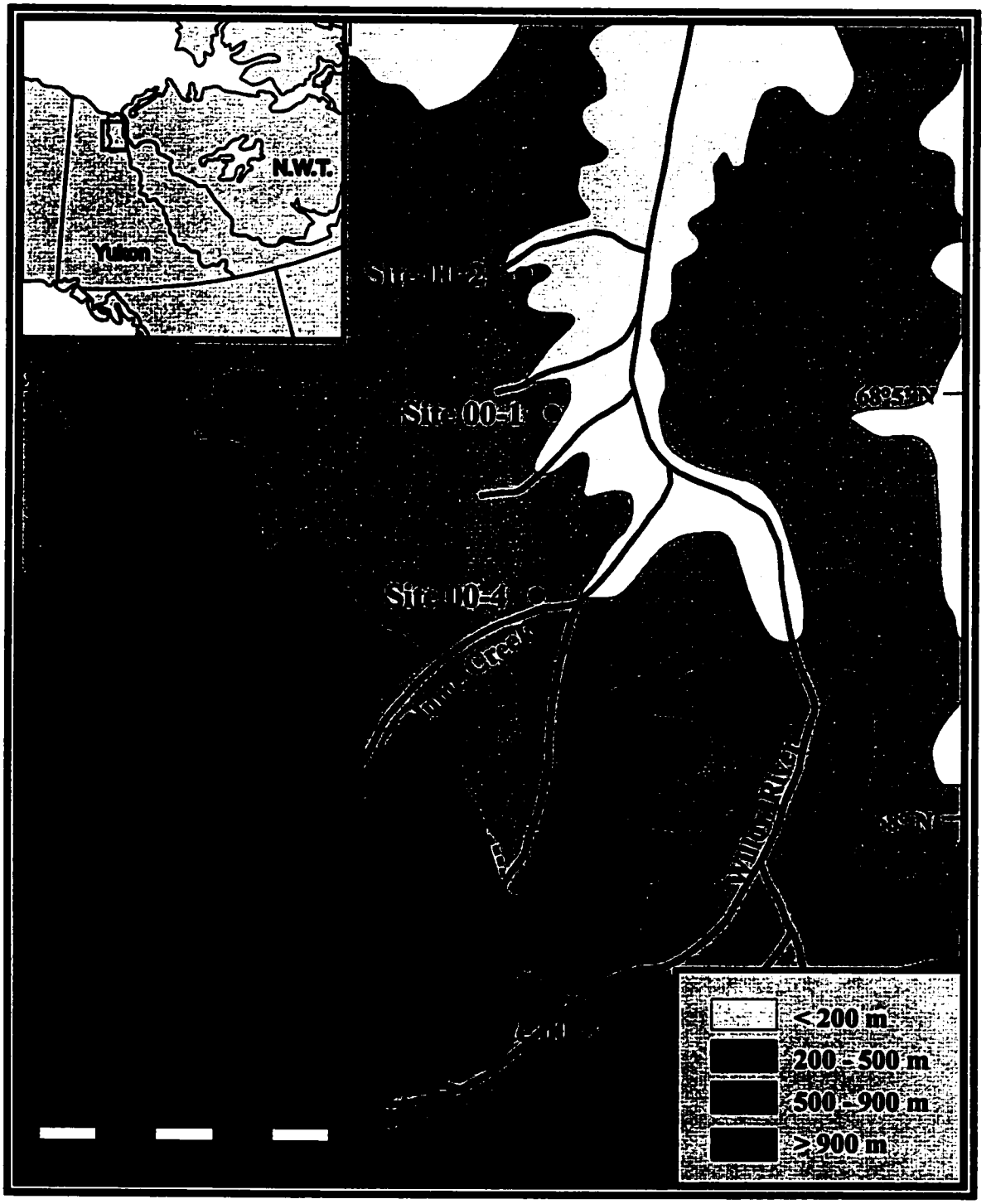

Figure 2.1: Location map of study sites in the Richardson Mountains, Northwest Territories. Dashed line represents maximum glacial extent during the Late Wisconsin. Note that site 00-2, includes thaw slumps 00-2A and 00-2B.

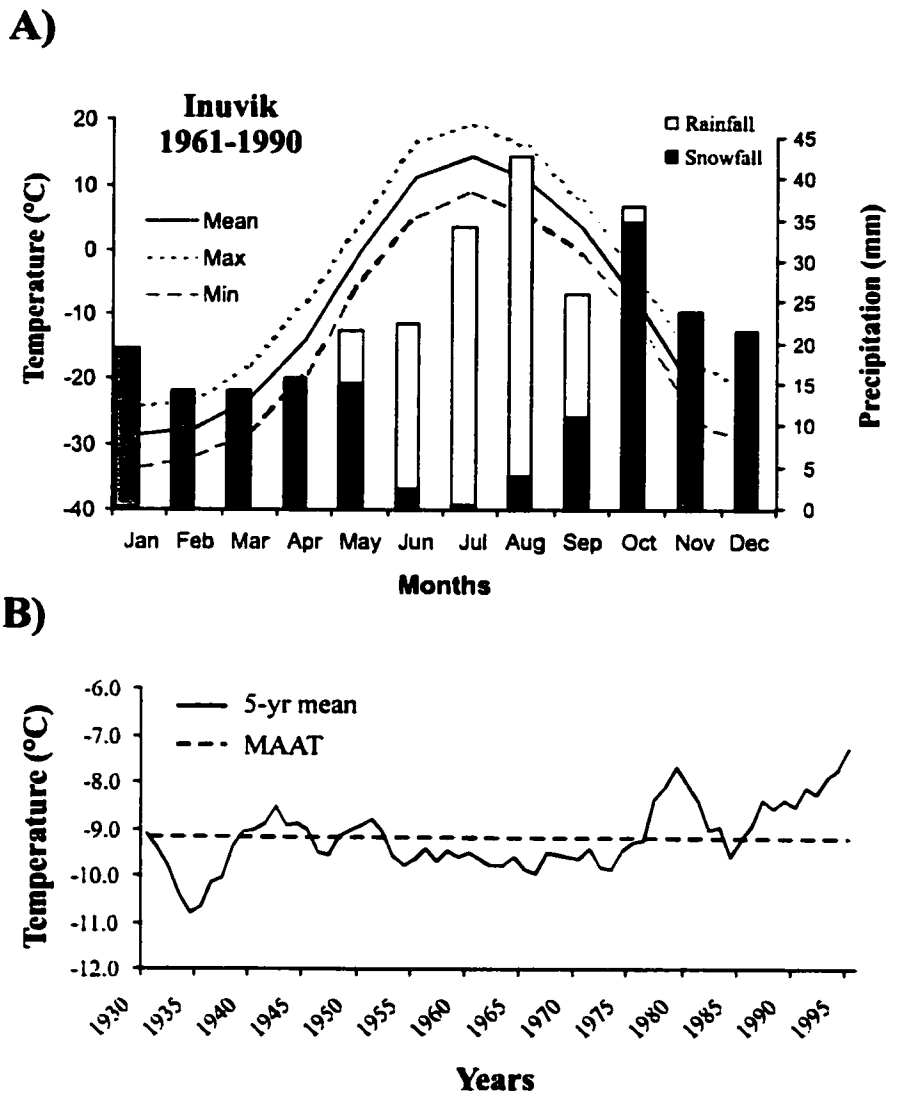

Figure 2.2: A) Normal monthly climate data recorded at Inuvik from 1961-1990. B) 5-year running air surface temperature trend recorded from Inuvik compared to mean annual air temperature. (Source: Environment Canada 2001).

2.5 METHODOLOGY

Fieldwork was undertaken from June 18th to July 5th 2000 within Willow River's drainage basin in the Richardson Mountains to examine tabular debris-rich ice exposed in retrogressive thaw slumps. The exposures present in the headwalls of thaw slumps were described, with special attention to the cryostratigraphy and sampled at every 30 cm intervals for isotopic composition and water (ice) content. At least 5 cm of material was removed from the thaw face before sampling to avoid possible contamination. It was unnecessary to maintain the samples in their frozen state for transport back to Ottawa for the determination of $\delta^{18}O$ and δD concentration in the ice. Buried organic material was collected from the headwall for radiocarbon dating (AMS).

Stable Isotope Analyses

Stable isotope analyses ($\delta^{18}O$ and δD) were conducted at the G.G. Hatch Isotope Laboratory at the University of Ottawa. The debris-rich ice samples were first allowed to equilibrate at room temperature in their sealed containers from which the supernatant water was extracted for analysis. The $^{18}O/^{16}O$ ratios was measured in CO_2 equilibrated with the water at 25°C on a VG SIRA-12 isotope mass spectrometer (analytical precision of ± 0.15‰). The D/H ratio was determined on a VG 602E mass spectrometer on samples converted to H_2 gas by reduction on metallic zinc in breakseals (analytical precision of ± 1‰). Results are presented using the δ-notation, where δ represents the per mil relative difference of $^{18}O/^{16}O$ or D/H in a sample with respect to the Vienna Standard Mean Ocean Water (VSMOW).

Gravimetric and Volumetric Water (Ice) Content

Two parameters are often used to describe ground ice conditions. First the gravimetric water content of a soil is defined as the mass of ice to dry soil, and is expressed as a percentage. Low ice content soils are generally regarded as those having gravimetric moisture content less than 40–50%. Massive ice bodies usually have ice content that average at least 250% for a thickness of several decimeters.

Volumetric water content is a second parameter commonly used in the description of ground ice and refers to the volume of ice as a proportion of the volume of the total sample. The advantage of this index is that it allows for the calculation of "excess ice" and thus provides some indication on the potential of volumetric ground loss upon thawing of permafrost. Volumetric ice content was measured using the method developed by Pollard and French (1980). The volume fraction of ice (fVi) of the frozen soil materials equals:

$$[1]\ fVi = Vi / (Vi+Vs)$$

where Vi is the volume of ice; and Vs is the volume of soil solids

$$[2]\ Vi = W + (0.09W)$$

where W is the weight of water

$$[3]\ Vs = \gamma d / Ps$$

and, where γd is the dry soil weight; and Ps is the particle density.

2.6 RETROGRESSIVE THAW SLUMPS

Retrogressive thaw slumps are among the most active geomorphological features in the Richardson Mountains. The thaw slumps are located within the margin of the late-glacial maximum westward extension of the Laurentide ice sheet (Figure 2.1), which occurred around 30,000 BP (Lemmen et al. 1994; Duk-Rodkin and Hughes 1992). The maximum glacial limit followed the northeastern front of the Richardson Mountains and moved northwest towards Herschel Island (Duk-Rodkin and Froese 2001). Beget (1987) concluded that the northwestern lobe of the Laurentide ice sheet was very thin (~200 m) during the Late-Pleistocene and that it was warm-based. Eskers in the study area also support a regionally warm-based condition of the ice sheet in the vicinity of Willow River.

Cryostratigraphy of exposed headwalls within thaw slumps

The thaw slumps are developed on plateaus ~100 m above Willow River and expose a 4 – 20 m high sub-vertical headwall in which 2 units were identified on the basis of ground ice structure: a debris-rich ice (Unit 1) overlain by a diamicton (Unit 2) (Figure 2.3). The slump floor is of low gradient (2° – 10°) (Figure 2.4) and covers an area of 300 m by 100 m. This zone is saturated with water originating from ice thawing in the exposed headwall and from surface runoff. On occasion, catastrophic mudflows develop from the slump floor and flow down the mountainside, which has slope between 8° and 20° (Figure 2.4). At the bottom of the slope, the sediments accumulate to form a debris cone, which blocks the bed of Willow River and increase its sediment load.

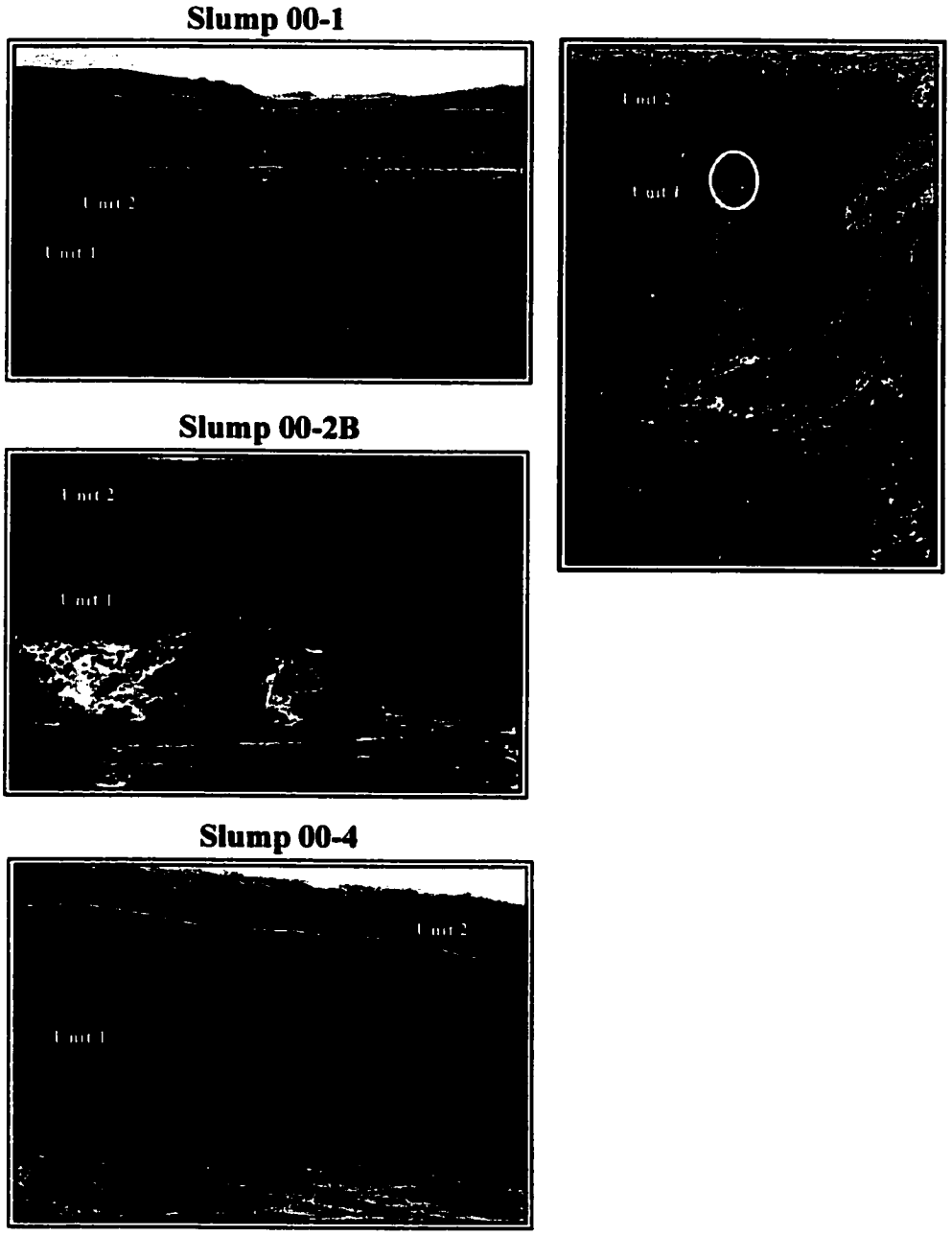

Figure 2.3: View of the diamicton (unit 2) and of debris-rich ice (unit 1) exposed in retrogressive thaw slumps. Note the numerous clumps of organic matter on the slump floor on the upper photograph and the formation of buttress at the base of the headwall in the lower photograph, which is the first sign of stabilization of the thaw slump. Circled person for scale.

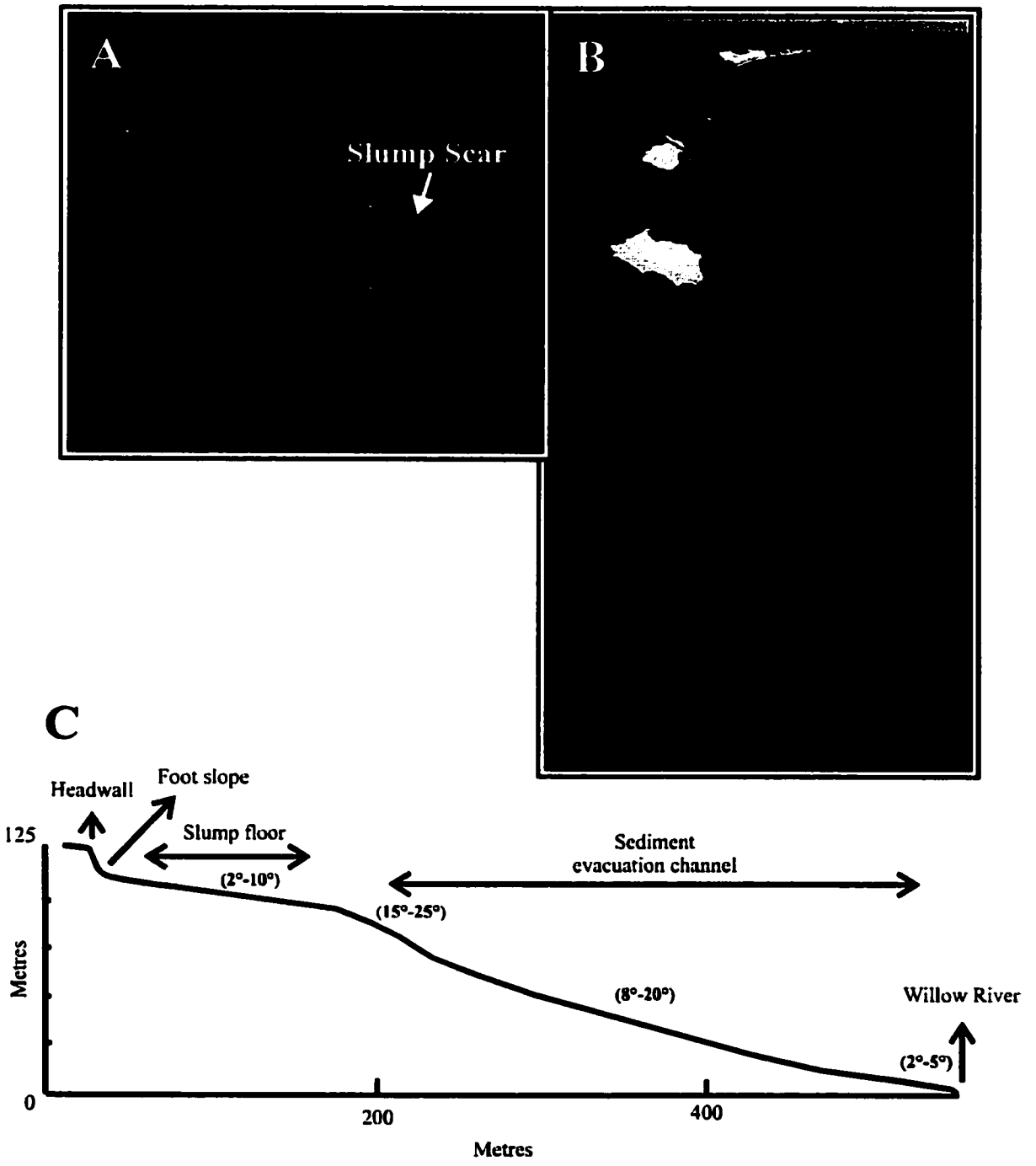

Figure 2.4: A) Visible slump scar located above the headwall of thaw slump 00-2A (in foreground). B) Oblique view and C) Topographic profile of a retrogressive thaw slump in the Richardson Mountains, NWT.

Unit 1: Debris-rich ice

Unit 1 consists of tabular debris-rich and exhibits sub-horizontal wavy bedding parallel to the ground surface (Figure 2.3). It is up 15 m thick and has a sharp erosional contact with the overlying icy diamicton (Unit 2). Since all of the studied thaw slumps are polycyclic in nature, it is not possible to rely on the nature of the upper contact as a criterion for the origin of the debris-rich ice (Mackay 1989). Lower contacts are rarely observed in retrogressive thaw slumps, as they are covered by slumping material. However, since rock-outcrops are visible, it is assumed that the Lower Cretaceous shale bedrock (Norris 1984) is only a few meters below.

The debris-rich ice (Unit 1) has a mean volumetric ice content of 70% (n = 31) on account of dispersed fined grained sediment, where 75% have a grain size < 63 μm; 15% are between 63 μm and 2 mm of diameter; and 10% have a grain size > 2 mm (Figure 2.5). Suspended cobble-to-boulder size clasts are rare in this unit. Some large ice nodules of several cubic decimeters are present. These nodules are transparent and contain many small spherical gas inclusions. Ice crystals from two samples were analyzed using a four axis universal stage (Langway 1958). They displayed euthedral to subhedral texture and are characterized by small to mediums grains (0.10 cm^2 to 4.35 cm^2) that averaged 1.25 cm^2 in area (n = 70) with no apparent preferred C-axis orientation (Figure 2.6).

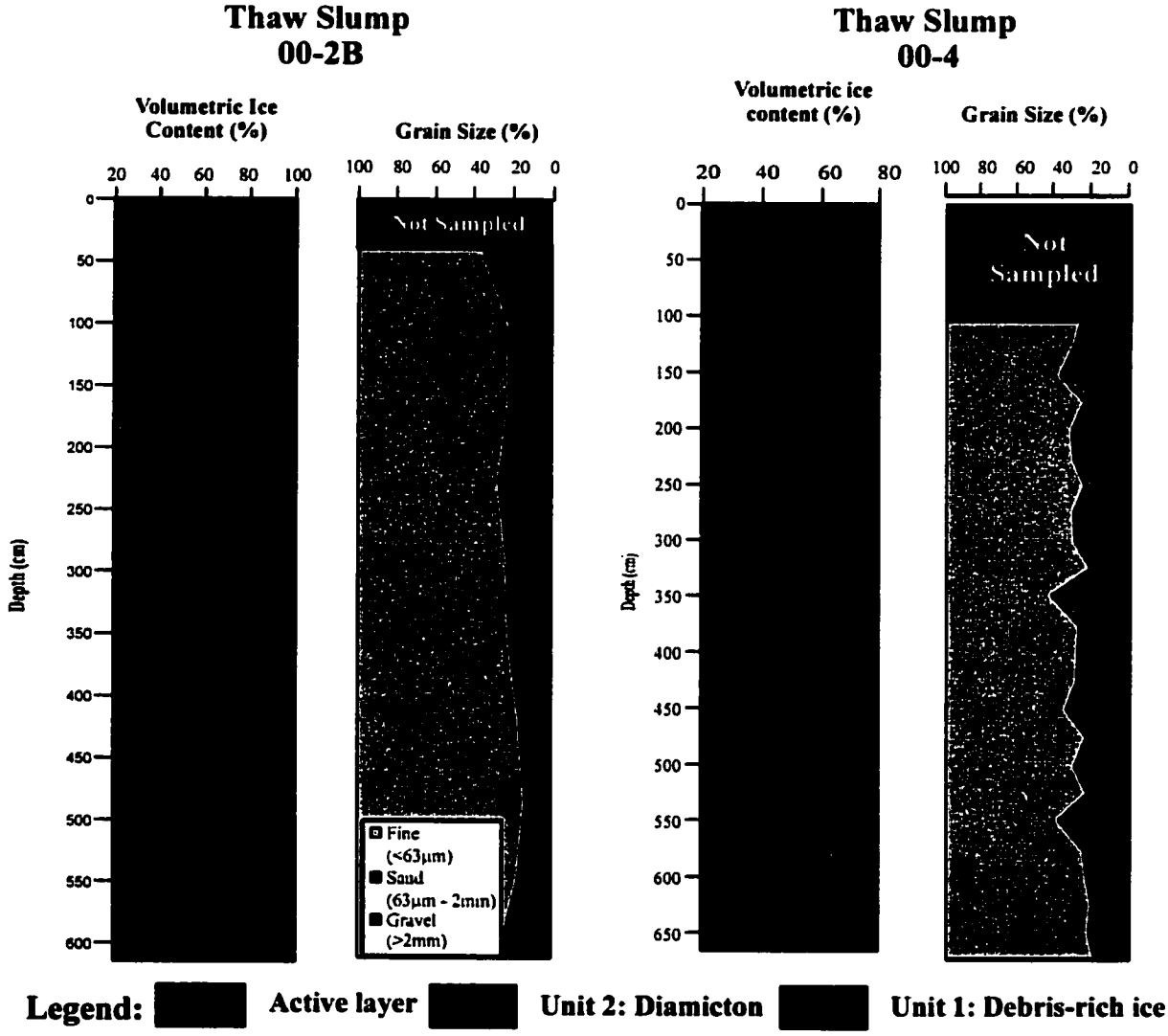

Figure 2.5: Volumetric water (ice) content and grain size profiles of thaw slump 00-2B and 00-4.

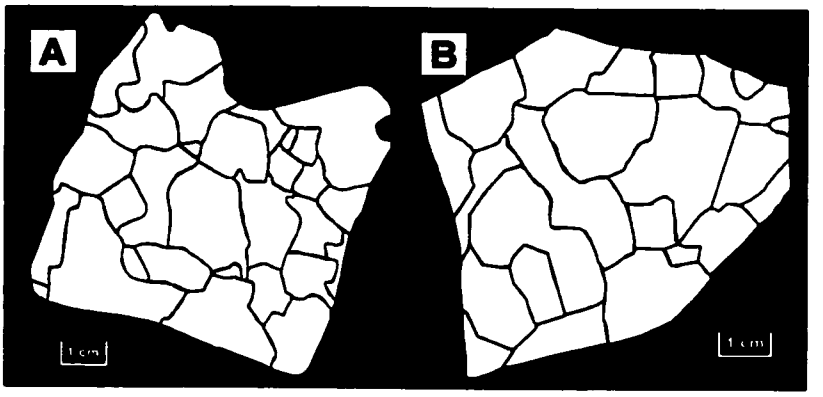

Figure 2.6: Tracing of thin sections from pure ice nodules found in the debris-rich ice. The ice crystals average 1.25 cm^2 in area.

Unit 2: Diamicton

The diamicton (unit 2) is up to 5 m thick. It has a regular reticulate ice structure near the lower contact which grades upward to a parallel-layered lenticular ice structure in the active layer. The mean volumetric ice content of this unit is 50% (n = 15) and the sediments consist also of mostly fines (70% fines; 18% sands; 12% gravel) (Figure 2.5). It is believed, from pebble lithological counts and granulometric analysis, that Unit 2 consisted of the same material as Unit 1, but was subsequently reworked by mass movements and surface processes. The active layer in the area is currently between 20 cm to 70 cm with a mean ground temperature around –3°C (Burn 2001).

Organic matter, mostly rhizomes, collected from unit 2 yielded radiocarbon ages from 8765 ± 230 BP to 150 ± 50 BP in which three periods of slumping activity were depicted (Table 2.1). The first and most important period is during the early Holocene, particularly around 8,500 BP to 8,000 BP. During this period the climate was much

warmer (3°C to 6°C) and wetter than today (Lauriol et al. 2002). The second period falls within the middle of the Holocene, between 4000 BP and 2000 BP, a cooler and drier period, with periodic warm episodes (Lauriol et al. 2001). The third period occurs during the last few centuries. It might be a result of increased temperature and/or precipitation in the region since the modern organic matter could have an apparent age of several centuries. The age determination suggests that the diamicton (Unit 2) is the result of many episodes of thawing, slumping and reworking activity throughout the Holocene and indicates that the debris-rich ice (Unit 1) has a minimum age of > 9,000 BP.

Table 2.1: Radiocarbon dates obtained from retrogressive thaw slumps in the western Canadian Arctic.

Time period	*Laboratory number*	*^{14}C Age (yr BP)*	*Methods*	*Material type*	*Site*	*Source*
Modern	TO-8890	150 ± 50	AMS	organics	00-1	this study
	TO-8891	270 ± 50	AMS	organics	00-2A	this study
	TO-8895	350 ± 50	AMS	organics	00-4	this study
	TO-8893	350 ± 50	AMS	organics	00-3	this study
Mid-Holocene	TO-8892	2040 ± 50	AMS	organics	00-2B	this study
	TO-8896	4230 ± 60	AMS	wood	00-2B	this study
Early Holocene	GSC-2305	7950 ± 280	Conv.	rhizomes		Burn, 1997
	TO-5889	8060 ± 70	AMS	rhizomes		Burn, 1997
	TO-8888	8120 ± 70	AMS	organics	00-1	this study
	TO-3608	8130 ± 70	AMS	rhizomes		Burn, 1997
	TO-8887	8180 ± 70	AMS	organics	00-1	this study
	TO-8894	8240 ± 70	AMS	organics	00-4	this study
	TO-8889	8560 ± 70	AMS	peat	00-1	this study
	GX-4352	8765 ± 230	Conv.	rhizomes		Burn, 1997

2.7 RESULTS

The isotopic composition of water (ice) provides a tool to distinguish between waters of different origins. For the purpose of comparison, the $\delta^{18}O$ composition of the Laurentide ice sheet was defined. Pleistocene age ice is outcropping along the margin of Barnes Ice Cap (Baffin Island) in a distinctive white band owing to the recession of the ice cap during the Holocene. Zdanowicz et al. (2002) suggested this white band, which has $\delta^{18}O$ values ranging from –42‰ to –26‰ with a mean $\delta^{18}O$ value of –33.1‰, is Laurentide ice. The Laurentide ice plots on a slope of 8.28 (Figure 2.7; $\delta D = 8.28\ \delta^{18}O + 16$), which is similar to the Global Meteoric Water Line (GMWL; $\delta D = 8\ \delta^{18}O + 10$; Craig 1961).

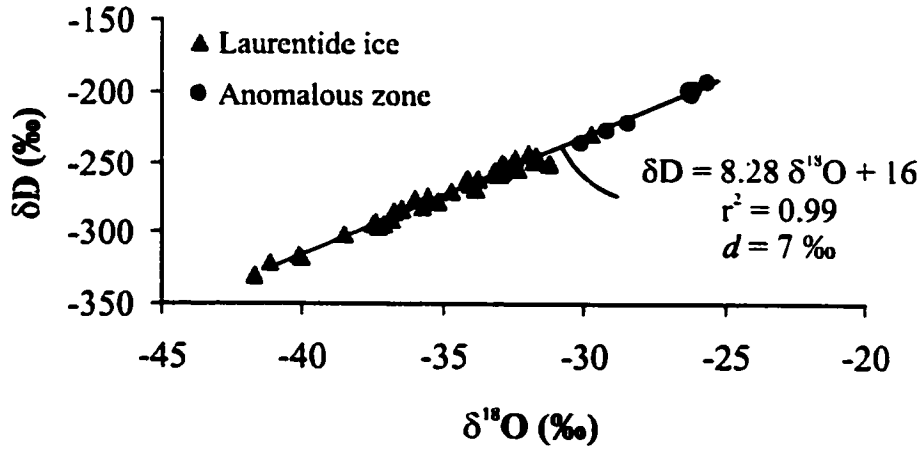

Figure 2.7: Co-isotope diagram showing the isotopic composition of Laurentide ice recorded in Barnes Ice Cap (data from Zdanowicz et al. 2002).

Thaw Slumps 00-2A and 00-2B

Thaw slumps 00-2A and 00-2B (68°06'N ; 135°39'W), separated by only a few meters, are located in the northern part of Willow River valley and most probably result from the ablation of the same ground ice body. The headwall of thaw slump 00-2A exposes 3 m of debris-rich ice (Unit 1) overlain by 1.5 m of diamicton (Unit 2) in which a radiocarbon date of 270 ± 50 BP (TO-8891) was obtained (Figure 2.8 A). The debris-rich ice is characterized by low $\delta^{18}O$ values ranging from –27.3‰ to –28.5‰ (n = 6) and plot on a slope of 6.44 ($\delta D = 6.44\ \delta^{18}O - 46$; $r^2 = 0.94$).

The headwall of thaw slump 00-2B exposes 4.5 m of debris-rich ice (unit 1) overlain by 2 m of diamicton (Unit 2). The $\delta^{18}O$ profile of thaw slump 00-2B (Figure 2.8 B) reveals an isotopic discontinuity at the contact between the debris-rich ice and the diamicton, which was dated at 2040 ± BP (TO–8892). The debris-rich ice has a mean $\delta^{18}O$ value of –28.9‰ ± 0.3‰ (n = 12), while the ice in the diamicton is characterized by $\delta^{18}O$ values ranging from –20‰ to –27‰ (n = 4), and plot on a slope of 9.22 ($\delta D = 9.22\ \delta^{18}O + 28$; $r^2 = 0.97$). It is not possible to obtain a reliable co-isotope slope for the debris-rich ice alone owing to their high degree of clustering. Nonetheless, the slope of the debris-rich ice of thaw slump 00–2B should be the similar to that of thaw slump 00–2A since they probably result from the ablation of the same ground ice body.

Thaw Slump 00-4

Thaw slump 00-4 (68°01'N ; 135°42'W) is located only a few hundred meters inside the maximum westward extension of the Laurentide ice sheet. It exposes 2.6 m of debris-rich ice (Unit 1) overlain by 2.5 m of diamicton (Unit 2). Organics found near the base of

the diamicton yielded a date of 8240 ± 70 BP (TO-8894). The $\delta^{18}O$ profile (Figure 2.8 C) shows no isotopic discontinuity at contact between the debris-rich ice and the diamicton. Instead the $\delta^{18}O$ values progressively increases upwards towards more enriched values through the erosional contact and continues to increase until the top of the profile is at the base of the active layer. The debris-rich ice is characterized by $\delta^{18}O$ values ranging from –25‰ to –29‰ (n = 26) and has a slope of 6.27 ($\delta D = 6.27\ \delta^{18}O - 48$; $r^2 = 0.75$). The $\delta^{18}O$ of the ice in the diamicton varies from –21‰ to –25‰ (n = 24) and has a slope of 7.90 ($\delta D = 7.90\ \delta^{18}O - 3$; $r^2 = 0.88$), which is similar to the Global Meteoric Water Line (GMWL; $\delta D = 8\ \delta^{18}O + 10$; Craig 1961).

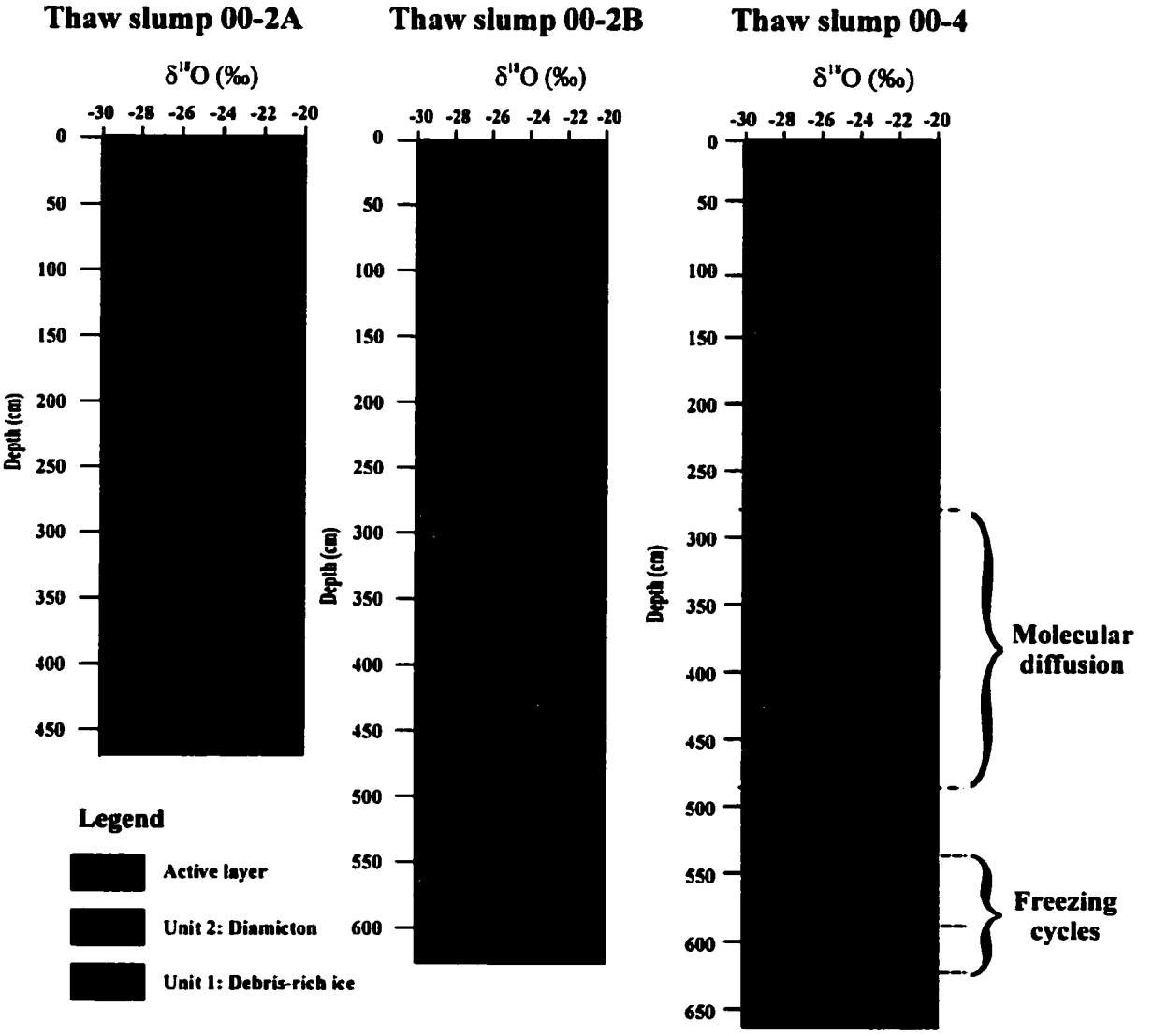

Figure 2.8: A) $\delta^{18}O$ profile from thaw slump 00-2A. A radiocarbon date of 270 ± 50 BP was obtained from rhizomes found in the diamicton. B) $\delta^{18}O$ profile from thaw slump 00-2B. A radiocarbon date of 2040 ± 50 BP was obtained from rhizomes found in the diamicton. C) $\delta^{18}O$ profile from thaw slump 00-4. A radiocarbon date of 8040 ± 70 BP was obtained from rhizomes found in the diamicton.

2.8 ORIGIN OF DEBRIS-RICH ICE

Background

Most massive tabular ground ice bodies in the western Canadian Arctic occur near the limits of known glaciations and different origins have been proposed (Lorrain and Demeur 1985; Mackay and Dallimore 1992). Currently, the most widely accepted theory of formation of massive ground ice bodies in the western Canadian Arctic is the one proposed by Rampton (1974; 1988*a*, 1988*b*). Rampton's model suggests that massive ground ice bodies are created from glacial meltwater driven to the glacier's terminus by a hydraulic gradient produced by the glacier's hydrostatic head of meltwater pressure in the fissured/crevassed melting margin of the ice sheet. The glacial advance caused permafrost to degrade below the ice sheet, thus opening taliks for subsurface meltwater flow (Clark et al. 2000). French and Harry (1990) proposed an alternative to the model in which the glacial advance would cause only the upper layers of a thick permafrost body to thaw near the ice margins and massive ground ice forming in the water-saturated till during retreat of the ice sheet.

The question surrounding the depth of thaw beneath the ice sheet is not fundamental to interpret our results. The impermeable shale (Norris 1984) constituting the bedrock, found at a shallow depth in the vicinity of Willow River, would have acted as an aquitard. Subglacial meltwater from the Laurentide ice sheet could have flowed through the till (open aquifer) between the glacier's sole and the bedrock surface.

There is now a growing tendency to interpret some massive ground ice bodies in western Canada as buried glacier ice (Lorrain and Demeur 1985; St-Onge and McMartin 1995). Glacier ice becomes buried during deglaciation by a debris overburden, which

may in continuous permafrost environments exceed the active layer thickness preventing the buried glacier ice from further thaw. Debris-rich basal ice has the best preservation potential because such ice would be quickly covered from summer thaw. However, since basal glacier ice results from multiple melting and refreezing episodes of meltwater at the glacier's sole, it may share some attributes (i.e. facies, water/ice chemistry) with segregated/injection ice making their differentiation difficult.

Origin of ice from $\delta D - \delta^{18}O$ systematic

The results of isotopic analyses from units 1 and 2 found in the headwalls of retrogressive thaw slumps are displayed on a co-isotope diagram and two distinct groups are depicted (Figure 2.9). Unit 1 is the most depleted in ^{18}O and D with a mean $\delta^{18}O$ and δD value of -28.2 ± 0.8 and -227 ± 7 respectively and plots on a slope of 6.84 ($\delta D = 6.84\ \delta^{18}O - 33$; $r^2 = 0.76$). Unit 2 is more enriched with mean $\delta^{18}O$ and δD values of -22.6 ± 1.8 and -181 ± 5 respectively and plots on a slope of 8.58 ($\delta D = 8.58\ \delta^{18}O + 12$; $r^2 = 0.94$). The highly negative ^{18}O values in the debris-rich ice are in the same range of ^{18}O values from Laurentide ice in the Barnes ice cap on Baffin Island (Figure 2.10) and from ice collected in Pleistocene sediment of the Tuktoyaktuk Peninsula (Mackay 1983). The ice in the Unit 2 is more enriched in ^{18}O and D indicating Holocene meteoric precipitation as an origin.

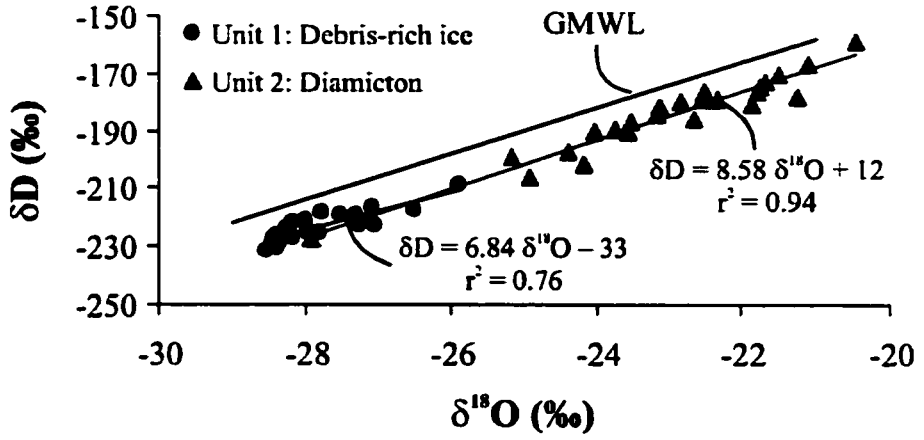

Figure 2.9: Co-isotope diagram showing the distribution of the ice in the diamicton and the debris-rich ice in all three thaw slumps studied in the Richardson Mountain. The Global Meteoric Water Line is given as a comparison.

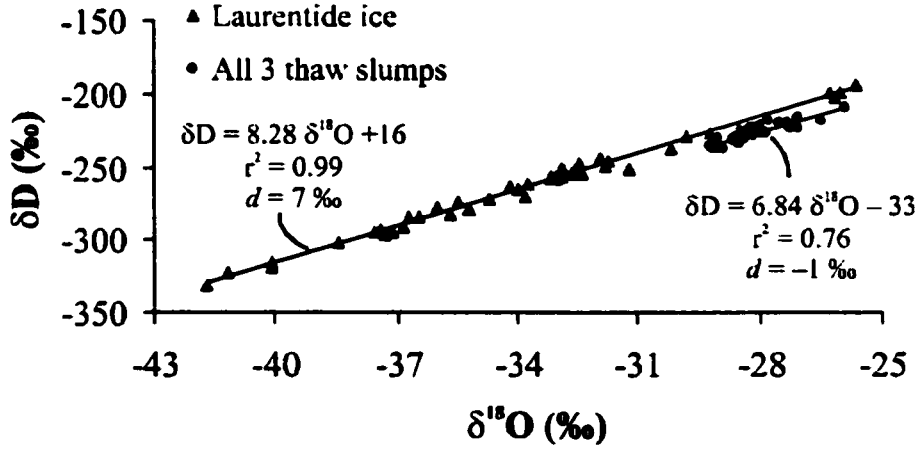

Figure 2.10: Co-isotope diagram showing the distribution of the debris-rich ice with respect to the Wisconsin ice recorded in the Barnes Ice Cap (Zdanowicz et al. 2002). The Wisconsinan ice has a deuterium excess value of 7‰, whereas the debris-rich ice has a deuteurium excess value of –1‰, indicating refreezing of meltwater.

Jouzel and Souchez (1982) showed that for a closed system freezing, where there is no input or output of water, the overall isotopic composition of the ice is derived from the isotopic composition of the initial water at the beginning of freezing and will plot on a slope no greater than six. A theoretical freezing curve has been calculated using Jouzel and Souchez's closed system model assuming an initial water composition of $\delta^{18}O = -34.1‰$; $\delta D = -266‰$. This initial water composition is the intersection point between the global meteoric water line and the observed freezing slopes of the debris-rich ice. The observed freezing slopes of the debris-rich ice ($S = 6.27$, thaw slump 00–4 and $S = 6.44$, thaw slump 00–2A) do not conform to the theoretical freezing slope ($S = 4.73$) obtained with the closed system model. Instead, the observed freezing slopes for the debris-rich ice are indicating freezing in a semi-closed or open system.

Moser and Stichler (1980) indicated that generally no fractionation occurs by melting glacier ice but is followed by enrichment in subsequent freezing. The meltwater issued from the Laurentide ice sheet would have a $\delta^{18}O$ and δD composition of –33‰ and –289‰ respectively. Contribution from local ambient precipitation would make these values slightly higher (~ –32‰). Freezing of meltwater issuing from the Laurentide ice sheet was calculated theoretically using a Rayleigh-like distillation with an equilibrium enrichment factor for water-ice exchange of $\varepsilon^{18}O_{i\text{-}w} = 3.1‰$ for ^{18}O and $\varepsilon D_{i\text{-}w} = 19.3‰$ for D (O'Neil 1968) (Figure 2.11). The model predicts an isotopic composition of the newly formed ice of –29‰ and –229‰ for $\delta^{18}O$ and δD and a theoretical freezing slope of 6.22 ($\delta D = 6.22\ \delta^{18}O - 49$) based on Rayleigh fractionation during freezing. The theoretical freezing slope ($S = 6.22$) is similar to the observed isotopic composition and freezing slope of thaw slump 00-2A ($\delta D = 6.44\ \delta^{18}O - 46$) and thaw slump 00-4 ($\delta D =$

6.27 $\delta^{18}O - 48$), which indicates that the debris-rich ice could have resulted from freezing of meltwater derived from the Laurentide ice sheet in an open system.

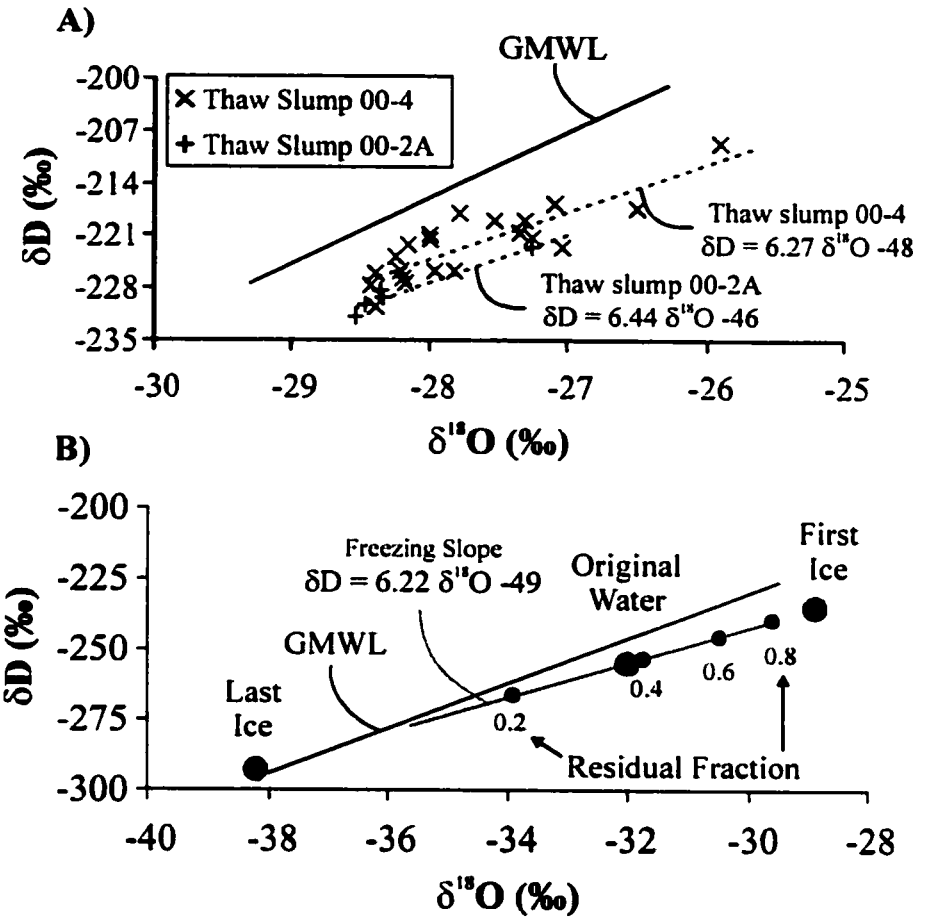

Figure 2.11: A) Co-isotope diagram showing the distribution of the debris-rich ice in thaw slump 00-2B and 00-4 with respect to the Global Meteoric Water Line. Thaw slump 00-2B has a measured freezing slope of 6.44 and thaw slump 00-4 has a slope of 6.27. B) Simulation of isotopic evolution of water issued from the Laurentide ice sheet during freezing using a Rayleigh-like distillation. The model predicts an isotopic composition of the newly formed ice of –29‰ and –229‰ for $\delta^{18}O$ and δD and a theoretical freezing slope of 6.22.

The freezing process results in isotopic fractionation because ^{18}O and D are preferentially incorporated into the solid phase (Figure 2.12). During the initial stage of freezing the ice will be isotopically heavier than the remaining water, but as freezing continues, each addition of newly formed ice will be isotopically lighter than the one before, owing to the removal of heavy isotopes in water. As a result, a freezing cycle could be represented by a downward gradation from isotopically heavy to isotopically light ice (Souchez and Jouzel 1984). There are a few single samples enriched by 2-3‰ in $\delta^{18}O$ in the debris-rich ice (Figure 2.8 C), which is characteristic of freezing at equilibrium (O'Neil 1968). These shifts are attributed to freezing of water during the downward migration of the freezing front thereby possibly indicating multiple injections of glacial meltwater and subsequent freezing during colder period. Generally, the bulk composition of the newly formed ice will be isotopically heavier than the initial water if some of the water is discharged without freezing (Clark and Fritz 1997).

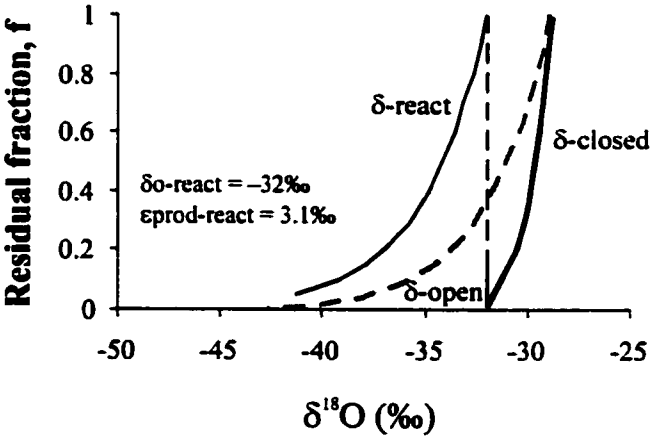

Figure 2.12: Rayleigh-like distillation of a water reservoir as it freezes to completion under (a) open system conditions represented by the δ-open curvve and (b) under closed system conditions represented by the δ-closed curve.

The measurement of the deuterium excess ($d = \delta D - 8\ \delta^{18}O$) was introduced by Dansgaard (1964) and can also give information on the origin of ice. The d excess is an indicator of non-equilibrium fractionation. On a global basis, *d*-value averages 10‰, but varies regionally due to variations in humidity (Dansgaard 1964). The *d* excess for the Wisconsinan precipitation recorded in the Barnes ice cap is equal to 7‰ and can be correlated to the moisture source of precipitation. The debris-rich ice (Unit 1) has a *d* excess of −1‰, indicating fractionation by melting and refreezing of meltwater (Figure 2.10). If the debris-rich ice were buried glacier ice, its *d* excess would be expected to be near 10‰. Thus, the low *d* excess seems to rejects a buried glacier ice origin for the debris-rich ice.

Possible explanation for the formation of the debris-rich ice

Stable isotopes analyses indicate that the debris-rich ice is derived from a cold paleo-water source, mainly glacial meltwater. The δD vs $\delta^{18}O$ diagram suggests freezing of glacial water in an open system and leaves two possible explanation for the origin of the debris-rich ice: 1*) Intrasedimental ice* or 2) *Buried basal glacier ice.*

A buried basal ice origin must not be neglected at this point, considering that the overlying and underlying material were not observed and that the possible freezing conditions deduced from δD vs $\delta^{18}O$ diagram may still reflect regelation conditions from an open system at the glacier's bed. As mentioned previously, it is often difficult to differentiate between segregated ice and basal glacier ice, which results from melting and refreezing of water at the glacier's sole, based on ice/water chemistry. Nonetheless, the

stratigraphic setting, $\delta^{13}C$ and CO_2 concentration of the debris-rich ice may lead to a possible conclusion on its origin.

The non-glaciotectonically deformed debris-rich ice seems to support an intrasedimental origin and warm-based condition of the ice sheet near its outer zone. In the study area, the Laurentide ice sheet advanced against the topography, which would have favored the development of internal deformation of the ice. If the origin of the debris-rich ice was buried basal glacier ice, one would expect the internal structure of the ice body to be different than parallel to the ground surface, as currently observed in the exposures.

Troutet (2002) carried out gas extraction (CO_2 concentration and $\delta^{13}C$) and $\delta^{18}O$ analysis on two ice nodules formed in the debris-rich ice at site 00-5. The ice nodules had $\delta^{18}O$ values of –29.1‰ and –27.6‰, which is comparable to the debris-rich ice (Unit 1). The CO_2 concentration in the ice nodules ranged from 56 μgC/kg ice to 128 μgC/kg ice (Table 2.2). Glacier ice, which encloses samples of air from the atmosphere at the time of bubble enclosure, shows very low levels of CO_2 concentration (34 μgC/kg ice). The CO_2 concentration is 3 to 9 times higher than the expected concentration in glacier ice from equilibration with the atmosphere. Soil gases usually have CO_2 concentration 10 to 100 times greater than the atmosphere. As plant material dies and degrades in the soil, microbial activity converts the carbon back to CO_2 in the soil (Clark and Fritz 1997).

The $\delta^{13}C$ values of the ice nodules ranged from –23.52‰ to –19.46‰ (Table 2.2) which is considerably more negative than the atmospheric CO_2 (~ –7‰). They are in the range of CO_2 produced by the decay of C_3 plants material, which usually has ^{13}C values between –26‰ to –20‰ (Clark and Fritz 1997). Carbon fixation by the leaf's

chloroplast results in an overall ^{13}C depletion of about 22‰ on the fixed carbon (O'Leary 1988). The CO_2 concentration and $\delta^{13}C$ values of the ice nodules in the debris-rich ice indicate that soil gases dominate the gases content in the ice and not atmospheric gases.

The physical and isotopic properties of the debris-rich ice (Unit 1) seems to indicate that the source of water for the debris-rich ice was most likely subglacial meltwater derived from the Laurentide ice sheet, which froze *in situ* during the downward permafrost growth.

Table 2.2: CO_2 pressure, concentration, and $\delta^{13}C$ values obtained from dry extraction of CO_2 from ice nodules found in the debris-rich ice at site 00-5. Agassiz ice cap samples (Arctic Canada) are given as comparison since they reflect atmospheric CO_2.

Lab No.	Sample No.	CO2 Yield[a] (mTorr/kg ice)	CO2 concentration[b] (µgC/kg ice)	$\delta^{13}C$ of CO_2 (‰ VPDB)	$\delta^{18}O$ of ice (‰ VSMOW)
B01-196-14	1er juil G1	5.44	128	-19.46	-27.61
B01-196-17	1er juil G2	1.95	56	-22.86	-29.12
B01-196-19	1er juil G3	4.12	83	-23.52	–
	87-1B*	0.32	34	–	–
	A84-82-5*	0.44	34	–	–
	76-1-B*	0.49	35	–	–

a = as measured at the pressure transducer
b = inferred from limit of calibration on equation range
* = Agassiz ice cap samples

Hypothesis of formation of debris-rich ice

The most probable interpretation of the origin of the debris-rich ice inferred from its physical and isotopic properties is that it has grown *in situ* by the freezing of water during downward permafrost growth. The isotopic composition of the debris-rich ice, as indicated by the highly negative $\delta^{18}O$ values (–30‰ to –27‰), suggests that the water source was meltwater issuing from the Laurentide ice sheet. The Richardson Mountains were ice covered around 30,000 BP – 25,000 BP and were ice-free by 21,000 BP (Duk-Rodkin and Hughes 1995). The interior of the north-western ice lobe of the Laurentide ice sheet is inferred to have been warm-based, given the observation of eskers and striations in the field and the reconstructed low glacier profile (Beget 1987). Downward freezing of sediment-charged meltwater in this proglacial aquifer is the likely origin of the debris-rich ice. Subglacial meltwater from marginal melting would have flowed under substantial pressure toward the glacier's terminus within water-saturated glacial sediments between the glacier's sole and the bedrock surface. Rapid retreat/thinning rates of the northwestern lobe of the ice sheet (Beget 1987) would most likely result in a decrease in hydrostatic pressure at the ablating margin of the ice sheet and in a decrease in subglacial meltwater fluxes. A decrease in subglacial meltwater flow from the ice sheet and a decrease in enthalpy transfer from the meltwater caused the freezing of the meltwater within the proglacial water-saturated till. Freezing of the subglacial meltwater, as it moved toward the freezing front into the water-saturated till, could have occurred periodically, perhaps even on a seasonal basis, as indicated by the freezing cycles in the debris-rich ice. A schematic diagram for the formation of tabular ground ice is presented in figure 2.13.

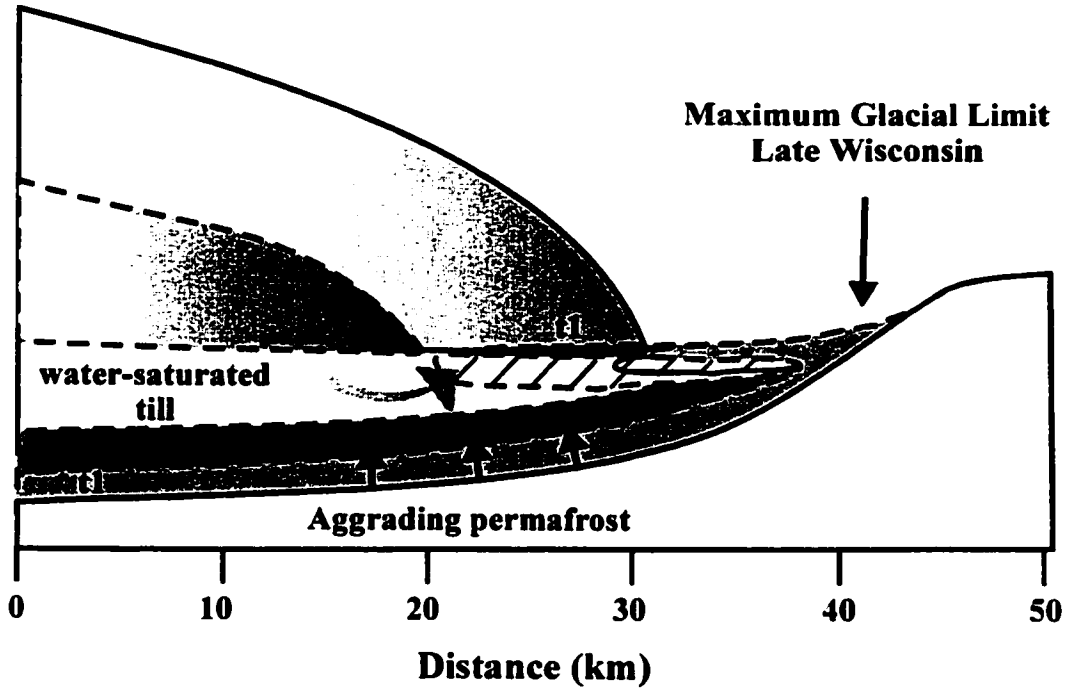

Figure 2.13: Schematic representation of the development of tabular ground ice through aggrading permafrost in the Richardson Mountains. Subglacial meltwater issued from the Laurentide ice sheet flowed through an aquifer between relict and aggrading permafrost. Rapid retreat/thinning rates of the ice sheet caused a decrease in meltwater flow, hence decreasing the latent heat transfer from the meltwater allowing the water to freeze *in situ* at the aggrading permafrost.

2.9 ORIGIN OF THE DIAMICTON ICE

The ice in the diamicton (Unit 2) is more enriched in ^{18}O and D (mean $\delta^{18}O$ and δD values of $-22.6 \pm 1.8‰$ and $-181 \pm 15‰$ respectively) and plots along a slope similar to the GMWL ($\delta D = 8.58\ \delta^{18}O + 12$) indicating Holocene meteoric precipitation as a main water source. As mentioned previously, temperature were 3 – 6°C warmer in northwestern Canada during the early Holocene (Ritchie 1984; Lauriol et al. 2002), which means that the precipitation would be up to 3‰ enriched in ^{18}O (~ –20‰) over modern precipitation (modern weighted mean $\delta^{18}O$ for Inuvik, –24‰; source: IAEA 1998). Geomorphological response to this warm period included a thicker active layer (Burn 1997) and greater thermokarst activity (Table 2.1). The maintenance of a thicker active layer over a prolonged period (i.e. millenniums) would allow for the replacement of lighter Pleistocene $H_2{}^{18}O$ (> –21‰) with heavier Holocene $H_2{}^{18}O$ waters (< –27‰). As a result, an isotopic discontinuity should be expected between the isotopically heavier diamicton ice and the isotopically depleted Pleistocene waters as is observed for thaw slump 00-2B. However, the isotopic shift is gradational over a 2 m section across the interface at site 00-4. The data suggest that isotopic evidence might not always be indicative of the thaw (erosional) unconformity. It is hypothesized that a thaw unconformity, generated by the maintenance of active layer depths considerably greater than today, will result in an isotopic discontinuity at the interface. This is corroborated by observation by Burn (1997) where an isotopic discontinuity exists at the regional depth of thaw during the early Holocene in the Mackenzie Delta. The isotopic shift might be progressive, if the thaw unconformity is a result of the development of retrogressive thaw slumps. Aggradation of permafrost occurs after the thaw slump

development ceases and would preserve the mixing profiles. Permafrost aggradation requires several decades to develop, as the rate of aggradation is sensitive to climatic variations (Burn 2000), which is relatively rapid compared to the early Holocene warm interval (10,000 BP to 7,500 BP).

The decreasing trend in the $\delta^{18}O$ profile of thaw slump 00-4 from the base of the diamicton (Unit 2) to 1.5 m into the debris-rich ice (Unit 1) (Figure 2.8 C) resembles that of a diffusion-dominated profile, which is now frozen (Figure 2.14). This conceptual model is currently being tested with a numerical model constructed by T. Birkham and J. Hendry (U. of Sask.). The profile in the diamicton is not consistent with mixing between Pleistocene meltwaters and Holocene precipitations, which would result in a linear mixing line (Clark and Fritz 1997). The development of a diffusion-dominated profile is a consequence of the change in climatic conditions that occurred after the last glaciation. Warm temperatures of the early Holocene replaced the cold temperatures of the Late Pleistocene, consequently allowing for the development of a former retrogressive thaw slump at that site. The newly formed active layer, 1 m in the floor of the former thaw slump, was quickly covered by meters of slumping Holocene material leaving a residual talik beneath the seasonally frozen layer. This depth of thaw is supported by a decrease in the volumetric ice content to 1 m in the debris-rich ice (Figure 2.5) and is consistent with the depth of paleo-active layers in the Mackenzie Delta (Burn 1997). During this time, the two endmembers diffused through the talik to form the lower diffusion profile that is presently observed in Unit 1 of thaw slump 00-4. The continuous addition of slumping material over the slump floor allowed for permafrost to aggrade through the talik (lower-diffusional section) in order to keep equilibrium with the surface air

temperature. The profile was most certainly truncated afterwards, since a small isotopic discontinuity is observed at the interface. The establishment of the lower-diffusion dominated profile most probably occurred between 8,500 BP and 7,500 BP after which permafrost would have aggraded to preserve to profile.

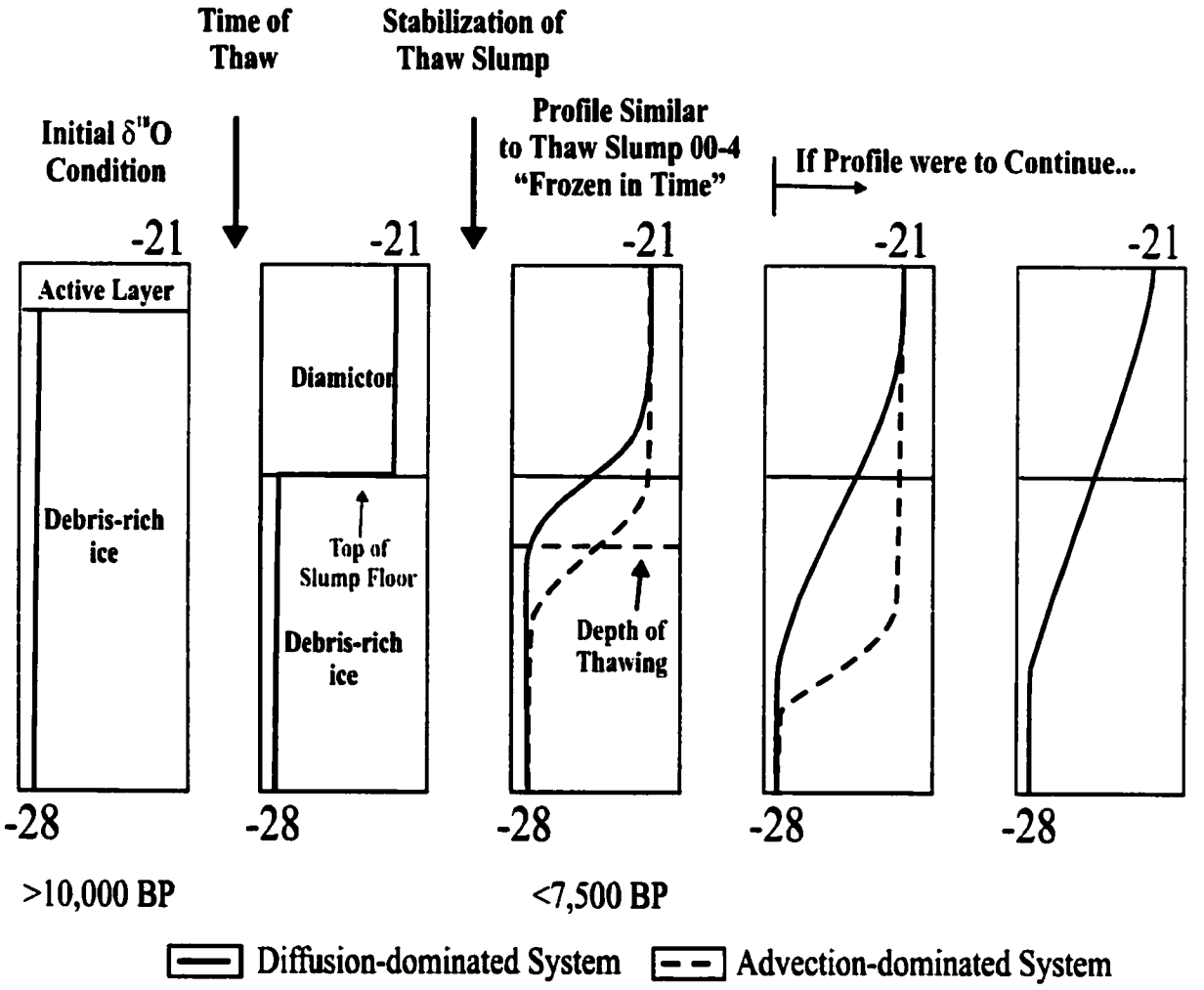

Figure 2.14: Conceptual model simulating the vertical transport of $\delta^{18}O$ in a diffusion-dominated system.

2.10 SYNTHESIS

An establishment of the chronology of the events that took place in the Willow River valley will allow for a better understanding of the Late Pleistocene glacial history of this region. The Laurentide ice sheet reached its maximum westward extension sometime around 30,000 BP to 25,000 BP (Lemmen et al 1994). During this advance, the Laurentide ice sheet caused the upper layers of a thick permafrost body to thaw, thereby enabling subglacial meltwater to flow through a talik formed between relict and aggrading permafrost. The meltwater froze *in situ* into the water-saturated till as a result of aggrading permafrost and decreasing meltwater fluxes. By 21,000 BP the ice sheet had retreated east of the Richardson Mountains allowing the development of a proglacial drainage system to enter the Beaufort Sea (Duk-Rodkin and Hughes 1995).

The climate warmed rapidly after 11,000 BP, as indicated by the intense thermokarst activity and by the important increase in active layer thickness in the western Canadian Arctic from 11,000 BP to 8,000 BP. During this very warm period (3°C to 6°C warmer than present), isotopically enriched Holocene precipitation (> –23‰) mixed with isotopically depleted Pleistocene meltwaters (< –27‰) producing the isotopically heavier ice in the diamicton. Water migrating downward into the thawed sediment section generated a diffusion-dominated profile between the two endmembers of the early Holocene precipitation and Pleistocene glacial meltwater.

The climate began to cool after ~ 8,000 BP allowing the freezing of the $\delta^{18}O$ profiles observed in the headwall of retrogressive thaw slumps. The occurrence of a diffusive-dominated $\delta^{18}O$ profile in a permafrost environment underlies the importance of a better understanding of groundwater movement in the continuous permafrost zone.

CHAPTER 3

CLIMATOLOGICAL AND HYDROLOGICAL CONTROL ON δD AND $\delta^{18}O$ OF METEORIC, SURFACE AND SUBSURFACE ICE IN THE NORTHERN YUKON

SUMMARY

δD–$\delta^{18}O$ analyses of meteoric, surface and subsurface waters (ice) were undertaken in the Northern Yukon. The results indicate that $\delta^{18}O$ is dependent upon a number of factors, such as surface air temperature, relative humidity and freezing rate. Holocene age waters are characterized by $\delta^{18}O$ values > –27‰, while Pleistocene age waters have $\delta^{18}O$ values < –27‰, indicating colder air surface temperature at the time of precipitation. The effect of evaporation on the isotopic composition of water follows a well-defined trend that is a function of relative humidity. This effect was best observed on open surfaces, such as shallow thermokarst lakes and active layer ice, where enrichments in the order of 5–11‰ in $\delta^{18}O$ were measured. The extent of fractionation is dependent upon the freezing rate. Slow freezing rates are usually accompanied with equilibrium fractionation. Isotopic fractionation should be observed during the formation of ground ice in the Northern Yukon, since gradual temperature changes are usually accompanied by slow freezing rates.

3.1 INTRODUCTION

Stable isotope variations (δD and $\delta^{18}O$) have been widely used to interpret past climatic conditions (Paterson et al. 1977) since the most inportant control on the isotopic composition of water is surface air temperature (Craig 1961). Any significant climatic variations will result in a change in concentration of the heavy isotopes in meteoric water. This relationship is due to the fact that decreasing temperature drives precipitation. Providing that no major isotopic changes occur by mixing, evaporation or fractionation, the $\delta^{18}O$ values for ice in permafrost should largely reflect air temperature at the time of freezing (Dansgaard 1964), and under favorable circumstances, permafrost stability and freezing history. Nikolayev and Mikalev (1995) have used samples from Siberia to correlate $\delta^{18}O$ variations with surface air temperature at the time of formation of ground ice. While, Michel and Fritz (1982) have shown that climatic change will result in a shift in the isotopic profile that is maintained for some depth, while isotopic fractionation during freezing will result in small scale positive shifts.

This chapter discusses the δD and $\delta^{18}O$ signatures of meteoric, surface, and subsurface ice in Northern Yukon. It provides a better understanding of the groundwater movement within the continuous permafrost zone and insights into the freezing history of ground ice.

3.2 REGIONAL SETTING

The study area is located in the Northern Yukon and covers approximately 50,000 km^2. It is mainly located in the Old Crow – Bluefish Basins, which lie in the middle of eastern Beringia, but also includes the Richardson, British and Barn Mountains (Figure 3.1). The Old Crow – Bluefish Basins are an ancient lowland with thick Quaternary accumulations of unconsolidated clays and silts capped by peat (Norris 1981). Permafrost is continuous (Brown 1974) and the active layer reaches ~ 30 cm in late summer in peatlands (Ovenden 1982). The area has a large number of thermokarst lakes, indicating poor drainage and high ground ice content

Climate

The Old Crow – Bluefish Basins have a continental subarctic climate characterized by cold, dry winters and short summers. Mean July temperature, derived from the Old Crow meteorological station is 14°C, while January mean temperature is –31°C (Figure 3.2 A; Environment Canada 2001). During the last 20 years, the surface air temperature has increased by 0.7°C (Figure 3.2 B). The total annual precipitation amounts to 250 mm, half of which falls as snow (Figure 3.2 A). Some precipitation is related to cyclonic activity, but in summer, rains frequently result from local advection phenomena (Wahl et al. 1987). In the hydrological atlas of Canada (1978), the Old Crow area is shown as having less than 200 mm of annual runoff, and less than 100 mm of annual evapotranspiration.

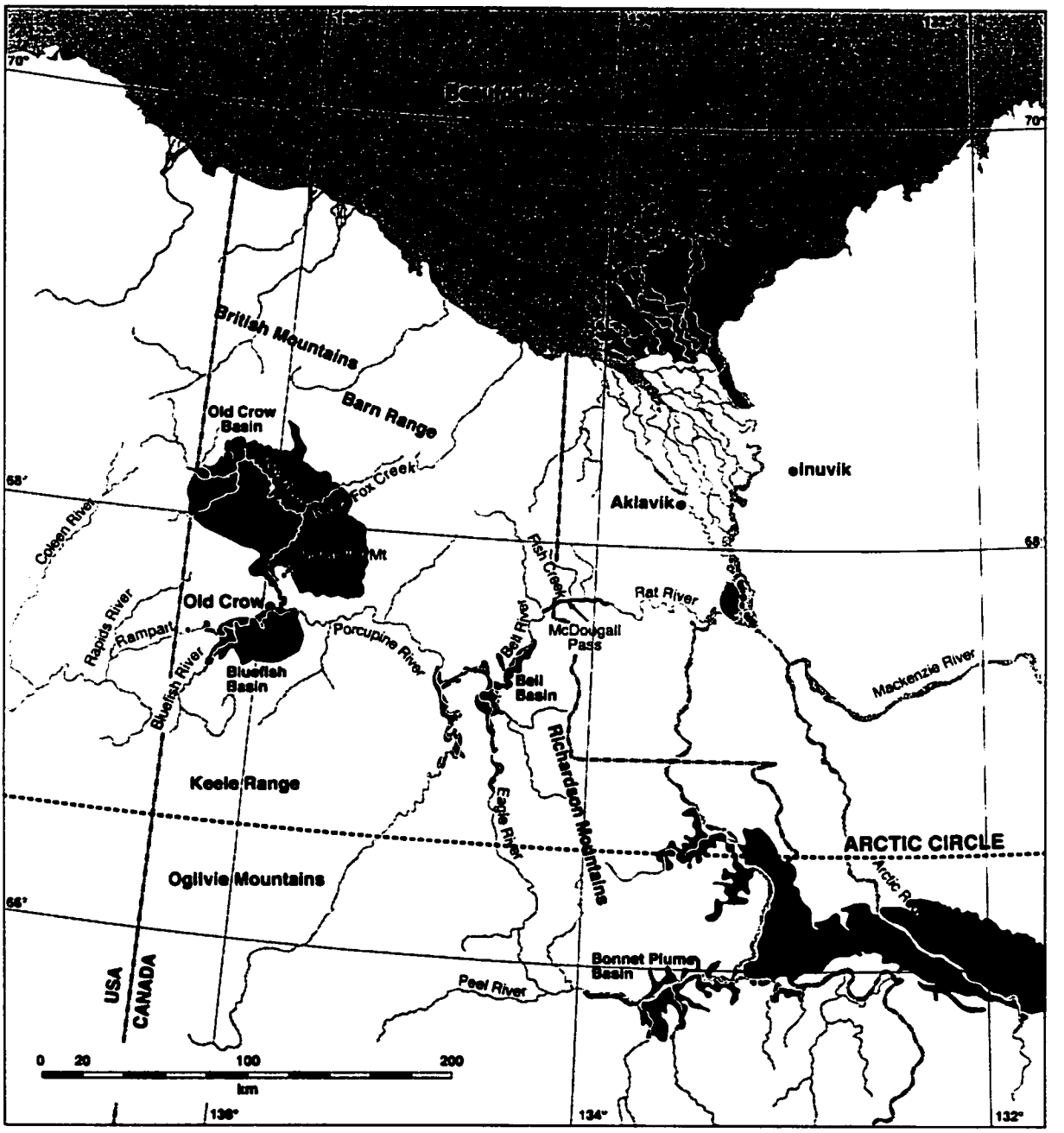

Figure 3.1: Location map of study area in the Northern Yukon with the major physiographic units.

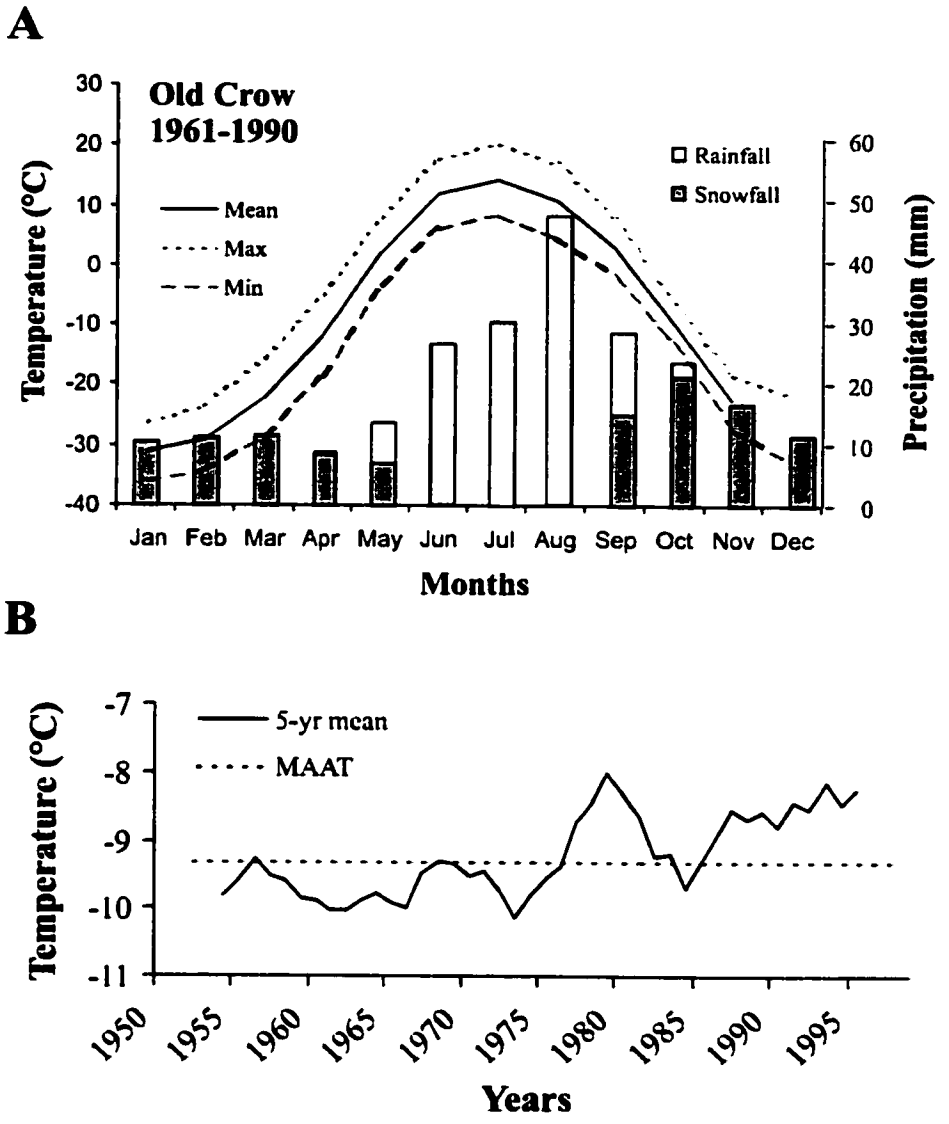

Figure 3.2: A) Normal monthly climate data recorded at Old Crow from 1961-1990. B) 5-years running average air surface temperature trend from Old Crow compared to the mean annual air surface temperature. (Source: Environment Canada 2001).

3.3 METHODOLOGY

This chapter includes unpublished data from thermokarst lakes, ice wedges and segregated ice that were collected by B. Lauriol and I.D. Clark during previous field seasons in the Northern Yukon, as well as data collected during the spring of 2001 in the Bluefish Basin, Yukon Territory. In the month of April of 2001, more than 25 cores were raised from "drained" thermokarst lakes. The frozen peat was cored by means of a modified SIPRE ice-corer, which is a motor-driven hollow drill with an inner diameter of 5.5 cm. The core was raised in 5-10 cm long segments, scraped to prevent contamination, and then placed frozen in high-density polyethylene bottles. The core segments were kept frozen until laboratory analyses were undertaken. Interstitial water was extracted from the frozen peat for $\delta^{18}O$ and δD composition. Two sub-samples were removed from Bluefish Core 1 (BF-1) for conventional radiocarbon dating at the Université de Laval. The samples dated were from the base of peat plateau, marking a transition from gyttja to the overlying peat accumulation and were from the middle of the core.

Analytical procedure

Stable isotopes analyses ($\delta^{18}O$ and δD) were conducted at the G.G. Hatch Isotope Laboratory at the University of Ottawa. Oxygen-18 was measured in CO_2 equilibrated with the water at 25°C on a VG SIRA-12 isotope mass spectrometer (IRMS), with an analytical error of ± 0.15‰. The D/H ratio was determined on a VG 602E mass spectrometer on samples converted to H_2 gas by reduction on metallic zinc in breakseals, with an analytical error of ± 1‰.

3.4 RESULTS

$\delta^{18}O$ signature of modern precipitation

A local meteoric water line (LMWL) has not been defined for the Old Crow – Bluefish region (67°58'N). Figure 3.3 depicts the linear relationship between $\delta^{18}O$ and δD of precipitation collected at Inuvik, NWT (68°30'N) from 1988 to 1989 (IAEA/WMO 1998) and at Mayo, YT (63°62'N) from 1985 through 1989 (IAEA/WMO 1998). Using a least squares fit, a LMWL has been defined for Inuvik:

$$[1] \qquad \delta D = (7.27 \pm 0.28)\, \delta^{18}O - (5.0 \pm 7.4);\ r^2 = 0.96$$

and, for Mayo:

$$[2] \quad \delta D = (6.27 \pm 0.31)\, \delta^{18}O - (37.4 \pm 6.8);\ r^2 = 0.93$$

Since the meteoric water line defined for Inuvik is only for 1 calendar year, it might not be totally representative of the isotopic composition of precipitation in the area. Nonetheless, it is very similar to the meteoric water line for Inuvik established by Vardy (1998) where the LMWL for Inuvik is: $\delta D = 7\, \delta^{18}O - 12$.

The $\delta^{18}O$ values from precipitation collected at Inuvik range from –35‰ to –16‰, and have a weighted mean $\delta^{18}O$ (n = 12) of –24.06‰ ± 0.82. While, the $\delta^{18}O$ values from precipitation collected at Mayo range from –28‰ to –10‰, and have a weighted mean $\delta^{18}O$ (n = 32) of –20.84‰ ± 0.37. The more negative $\delta^{18}O$ values are located at higher latitudes, which is coherent with the latitude effect observed by Dansgaard (1964). Since Arctic stations are located at the end of the Rayleigh rainout process, the $\delta^{18}O$–T gradient becomes increasingly steeper. The distribution of precipitation data along the

LWML's likely reflects the origin of the air masses, and the seasonality of precipitation. The measurement of the deuterium excess (*d* ‰) can provide information on the origin of the vapour masses. On a global basis, *d* excess averages 10‰, but varies regionally due to variations in humidity (Dansgaard 1964). Low *d* excess are characteristic of high humidity regions or might be indicative of secondary evaporation (Clark and Fritz 1997). Table 3.1 gives the weighted mean $\delta^{18}O$ values and *d* excess for Inuvik and Mayo. The *d* excess recorded at Inuvik is equal to 13.2‰, whereas at Mayo, it is equal to 3.3‰. The low *d* excess for Mayo is associated with strong seasonal differences, and reflects secondary evaporation effects during the summer months. Arctic stations are influenced by Arctic air mass, which barely brings moisture inland, except locally during the summer months. Consequently, Arctic stations have a lower δD–intercept due to evaporation effect during rainfall, giving slopes and δD–intercept lower than the GMWL.

Table 3.1: Weighted mean $\delta^{18}O$ values and *d* excess for Inuvik and Mayo. (Source: IAEA/WMO 1998).

Location	$\delta^{18}O$ (‰)	*d* (‰)
Inuvik	-24.1	13.2 ± 5.7
Mayo	-20.8	3.3 ± 7.9

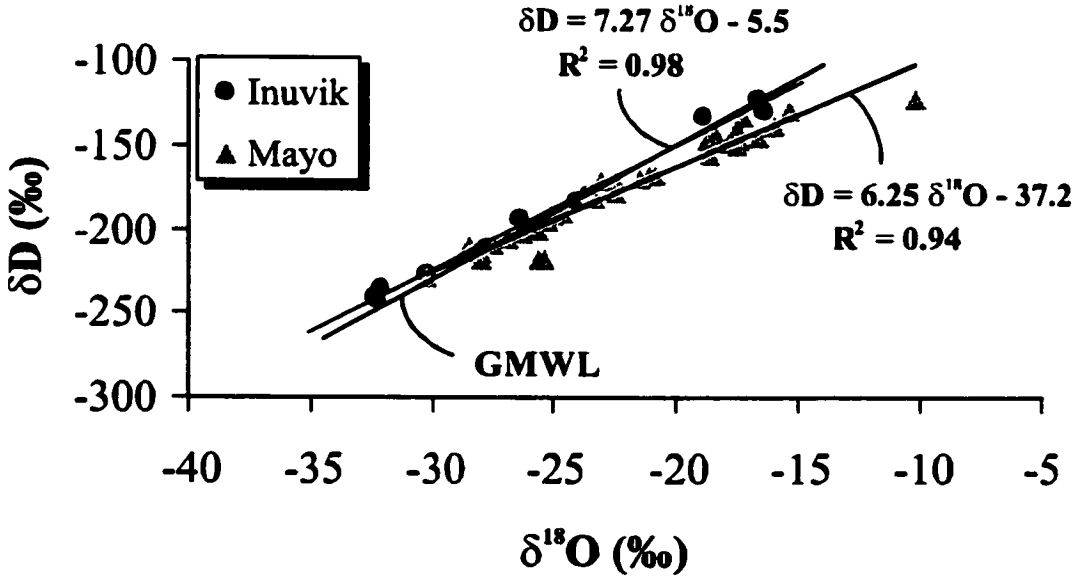

Figure 3.3: $\delta^{18}O$ vs δD diagram of precipitation collected at Inuvik (1988-1989) and at Mayo (1985-1989) (Source: IAEA/WMO 1998). The GMWL is given for comparison.

$\delta^{18}O$ signature of thermokarst lakes

Thermokarst lake waters, collected during the summer of 1998, are characterized by an enriched isotopic composition (–11.2‰ to –14.5‰) with respect to the weighted mean $\delta^{18}O$ recorded at Inuvik (–24‰). They plot below the LMWL on a slope of 4.8 ($\delta D = 4.8\ \delta^{18}O - 63$; $r^2 = 0.97$). A strong enrichment is observed in both ^{18}O and D, and if the isotopic composition of the lakes is regressed to determine their original isotopic composition ($\delta^{18}O = -22.2‰$ and $\delta D = -167‰$), enrichment in the order of 8‰ to 11‰ is observed. Gonfiantini (1986) showed how relative humidity and temperature largely influences ^{18}O and D concentration during evaporation, as the remaining water becomes progressively enriched in heavy isotopes following a Rayleigh-type distillation, and that, under conditions of increasing humidity, exchange with the vapour phase reduces the kinetic enrichment (Figure 3.4 A). On a δD–$\delta^{18}O$ diagram, this causes a deviation from the global meteoric water line along a line with a lower slope (Figure 3.4 B). It can be seen that for very low relative humidity, the slope will be close to 4, whereas for relative humidity closer to 75%, the slope is close to 5. As evaporation proceeds in low-humidity regions, such as the Old Crow region, the isotopic composition of the remaining water will become progressively enriched in heavy isotopes. Such a situation has been examined for the isotopic composition of thermokarst lakes in the Bluefish Basin (Figure 3.4 C). To calculate the average evaporative loss of a region, the local "evaporation slope" must be know or assumed. This slope is a function of humidity and temperature and was examined theoretically using Gonfiantini's equations. Total annual precipitation recorded at Old Crow meteorological station amounts to 250 mm/yr, while the evapotranpiration in the Old Crow region is less than 100 mm/yr (Hydrological Atlas of

Canada 1978). Giving that the effective moisture (precipitation – evaporation) in the Old Crow region is considered to be 60% (h = 0.6), and that the overall enrichments ($\varepsilon_{total} = \varepsilon_{v\text{-}l} + \Delta\varepsilon_{v\text{-}bl}$) for evaporation under these conditions are –14.98‰ for ^{18}O and –81‰ for D, then a theoretical evaporation slope of 4.6 ($\delta D = 4.6\ \delta^{18}O - 68$) is computed. This evaporation slope is similar to the observed slope of the thermokarst lakes ($\delta D = 4.8\ \delta^{18}O - 61$). Small and shallow thermokastic lakes will be most subject to significant evaporation. For these lakes, the isotopic composition is controlled by the humidity conditions and could be used as a proxy for effective moisture.

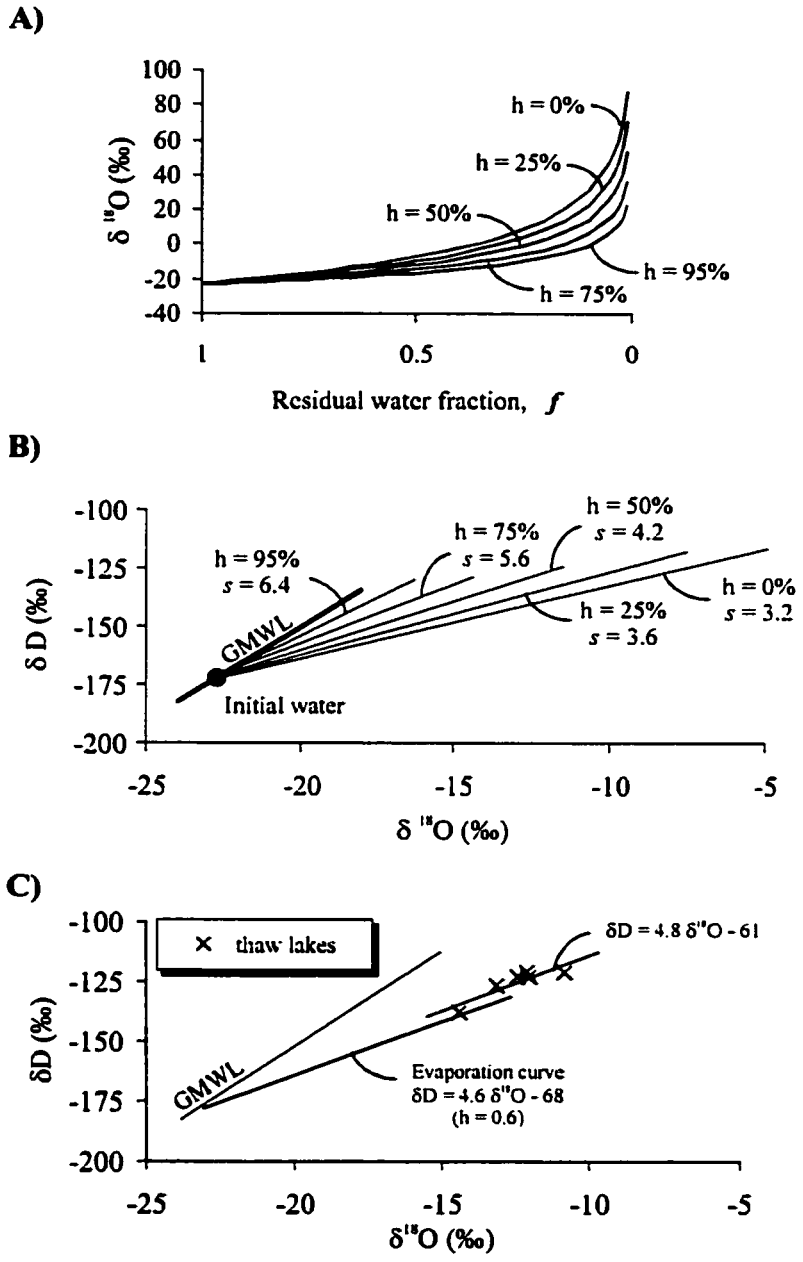

Figure 3.4: A) Enrichment of ^{18}O and D in water during evaporation. Under conditions of increasing humidity, exchange with the vapour phase reduces the exponential enrichment. B) Isotopic enrichment in evaporating water and the effect of humidity (from Clark and Fritz, 1997). C) The effect of humidity in evaporating thermokarst lakes in the Old Crow area compared to the calculated evaporation curve in the Old Crow Basin.

$\delta^{18}O$ signature of active layer ice

Active layer waters were extracted from the upper 30 cm of peat in 12 drained thermokarst lakes in the Bluefish Basin (Figure 3.5). They are characterized by an heterogeneous $\delta^{18}O$ composition ranging from –22.6‰ to –11.7‰, with an average $\delta^{18}O$ composition of –19.3‰ ± 0.8 (Table 3.2). This range of isotopic composition indicates that the active layer waters are mostly fed by rainfall (–23‰ < $\delta^{18}O$ < –16‰), and may receive additional water from late lying snowbanks and/or water released by basal thaw of the active layer. This is in agreement with results presented by Boike and Hubberten (1998) and Mackay (1983), who indicated that the main water sources for active layer water are meteoric rain and snowmelt water. However, on a δD–$\delta^{18}O$ diagram the active layer waters in the Bluefish Basin plot below the GMWL (Figure 3.6), indicating that they are influenced to some extent by kinetic fractionation. The slope of the active layer waters ($\delta D = 4.9\ \delta^{18}O - 64$; $r^2 = 0.88$) is similar to the calculated theoretical evaporation curve ($S = 4.6$) in the Bluefish Basin indicating that the ^{18}O and D concentration on open peat surfaces are controlled by relative humidity. The dry summers and lack of vegetation on some newly formed peat surfaces (Figure 3.7) could produce an enrichment in ^{18}O and D. This might cause an important spatial variability in the $\delta^{18}O$ composition of peat surfaces, depending on relative humidity and the vegetation conditions at the site.

Figure 3.5: Location map showing sampling points of active layer ice in the Bluefish Basin. Also shown is the location of a core (BF-1) retrieved from a peat plateau.

Table 3.2: $\delta^{18}O$ and δD variations of active layer ice in the Bluefish Basin.

	Isotopic variations of porewater extracted from the active layer												
	Stations												
	3	*4*	*5*	*6*	*8*	*9*	*10*	*12*	*13*	*14*	*16*	*23*	*Mean*
Mean $\delta^{18}O$	-15.3	-19.5	-20.0	-16.1	-19.2	-19.8	-19.5	-21.3	-21.5	-21.7	-16.0	-21.3	*-19.3*
Mean δD	-137	-158	-161	-141	n.a.	n.a.	-155	-171	-173	-172	-153	-177	*-160*
$\delta^{18}O$ *Variance*	0.32	0.50	0.10	0.21	0.01	0.10	0.00	0.28	1.33	1.29	14.18	0.02	*1.5*
$\delta^{18}O$ *Std. Dev.*	0.57	0.71	0.31	0.45	0.12	0.31	0.04	0.53	1.15	1.14	3.77	0.13	*0.8*
n	3	3	3	3	3	3	3	3	3	3	3	3	

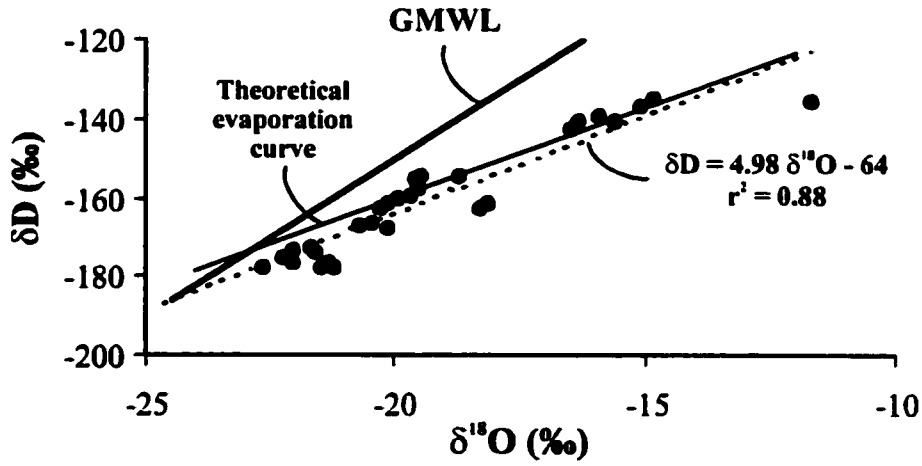

Figure 3.6: $\delta^{18}O$-δD diagram of active layer ice extracted from drained thermokarstic lakes in the Bluefish Basin compared to the theoretical evaporation curve measured for the area. The GMWL is given for comparison.

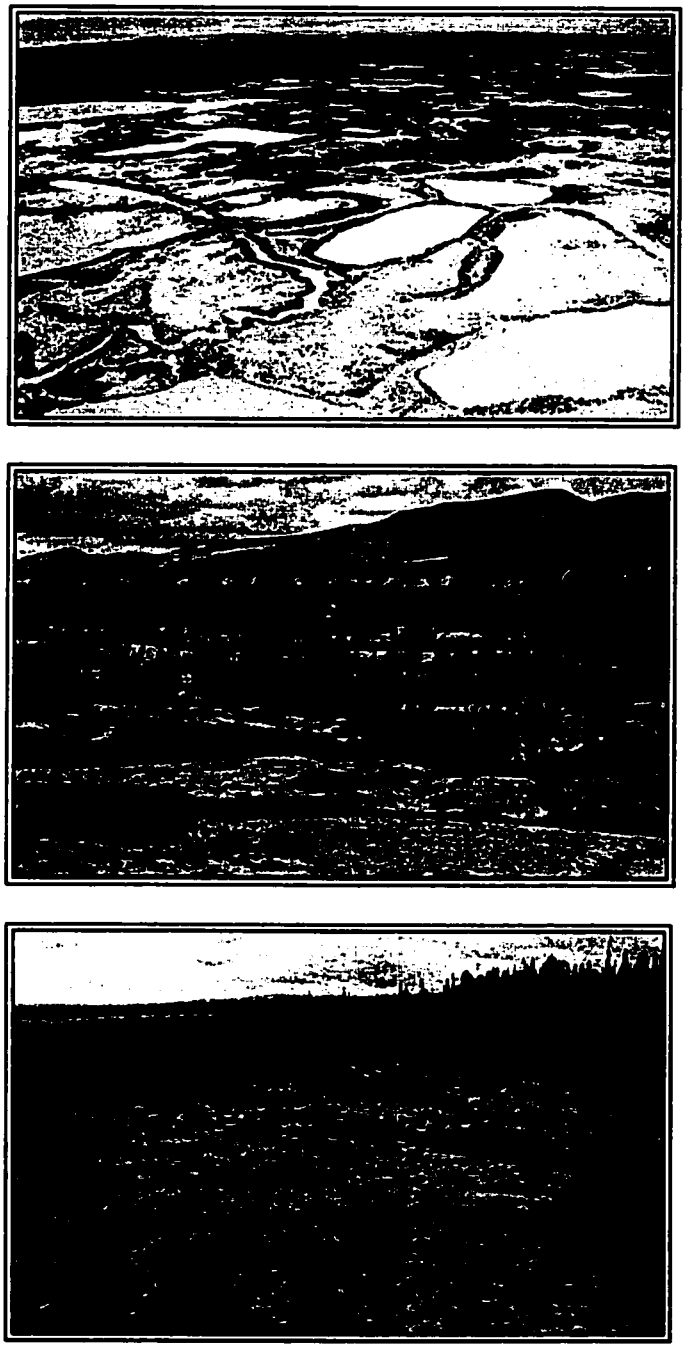

Figure 3.7: Photograph showing drained thermokarst lakes and lack of vegetation on these surfaces.

$\delta^{18}O$ signature of ice wedge ice

Isotopic variations within and between ice wedges from 3 sites located in the western Canadian Arctic (Chijii'Bluff and the Rampart of the Porcupine in the Bluefish Basin and at site 00-3 in Willow River in the Richardson Mountains) were examined. The ice wedges are all thought to be of Holocene age and their $\delta^{18}O$ compositions are plotted in figure 3.8. The range in $\delta^{18}O$ values (–29‰ to –22‰) agrees well with the range for modern ice wedge ice (–26‰ to –22‰) in the Tuktoyaktuk Peninsula (Mackay 1983; Michel 1990).

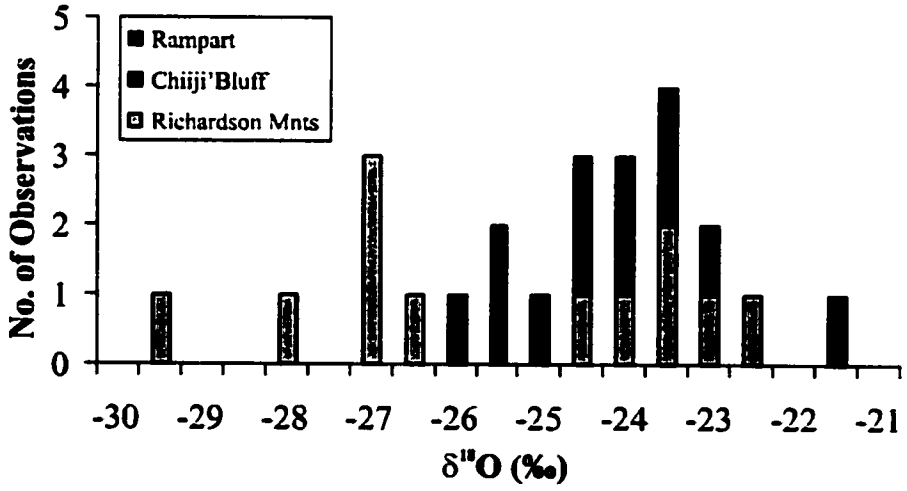

Figure 3.8: Histogram of $\delta^{18}O$ values of ice wedges located in the Richardson Mountains, from Chiiji'Bluff and from the Rampart of the Porcupine in the Bluefish Basin. Increments are 0.5‰.

Detailed $\delta^{18}O$ and δD analyses were completed on an ice wedge located in the Richardson Mountains (Figure 3.9). The anti-syngenetic ice wedge measured 2 m in height and 150 cm wide. A radiocarbon age obtained at the base of the ice wedge (8240 ± 70 BP; TO-8894) indicates that it formed during the Holocene. Due to the size of the samples, each sample represents a composite of several distinct near vertical ice layers of ice wedge ice since thermal contraction cracks rarely exceed millimeter width (Mackay 2000). The $\delta^{18}O$ values from this anti-syngenetic ice wedge range from –29‰ to –22‰ and show a gradual decrease in $\delta^{18}O$ values with depth with the exception of one sample located at the top left portion of the ice wedge. An anti-syngenetic ice wedge grows downward due to removal of slope material by mass wasting or erosion (Mackay 1990b). In an anti-syngenetic ice wedge, the ice on the sides increases in age from bottom to top (Figure 3.10). Therefore, the low $\delta^{18}O$ value (–26.07‰) obtain in the upper left portion of the ice wedge and near its base (–29.28‰ to –26.87‰) could have been obtained during an older and colder period, in which the thermal contraction cracks could have been deeper.

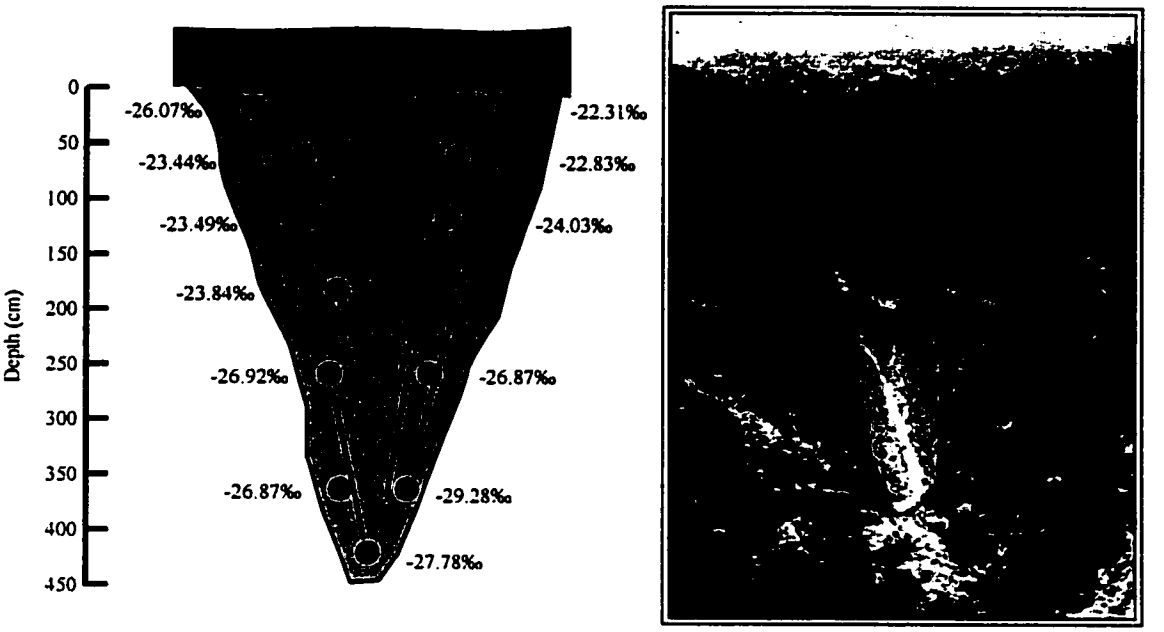

Figure 3.9: $\delta^{18}O$ composition of an anti-syngenetic ice wedge located at site 00-3 (Figure 2.1) in the Richardson Mountains.

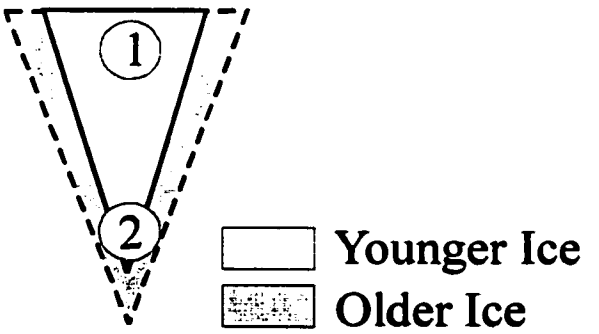

Figure 3.10: Schematic diagram showing the downward growth of anti-syngenetic ice wedge. In this type of ice wedge, the ice is oldest on the sides and increases in age from bottom to top.

Several researchers (Washburn 1980; Lauriol et al. 1995) have indicated that the primary source of water for ice wedge growth is derived from snow meltwater. Isotope exchange occurs during melting of a snow pack between meltwater infiltrating the snowpack and the snowpack itself, causing an isotopic enrichment (Clark and Fritz 1997). Using this characteristic, Lauriol et al. (1995) showed that the ice wedge ice formed during the last stage of snowmelt, since the first water to exit the snowpack would be more depleted than the original snow and located above the GMWL (Figure 3.11 A). The last water to exit the snowpack is enriched with respect to the original snow and located below the GMWL. The isotopic composition of the 3 ice wedges studied is consistent with this model (Figure 3.11 B). Since the $\delta^{18}O$ values are depleted (–26‰ to –22‰) with respect to summer precipitation (–22‰ to –18‰) and located below the GMWL, it is assumed that the water forming the ice wedge is derived from melting of residual snow.

The three distinct slopes on which the ice wedges are aligned are caused by distinct environmental conditions. Ice wedge growth is primarily controlled by snow meltwater issuing from a snowpack. The isotopic composition of snowpacks might differ from one site to another, depending on the interaction with the surrounding vegetation, topography and climate.

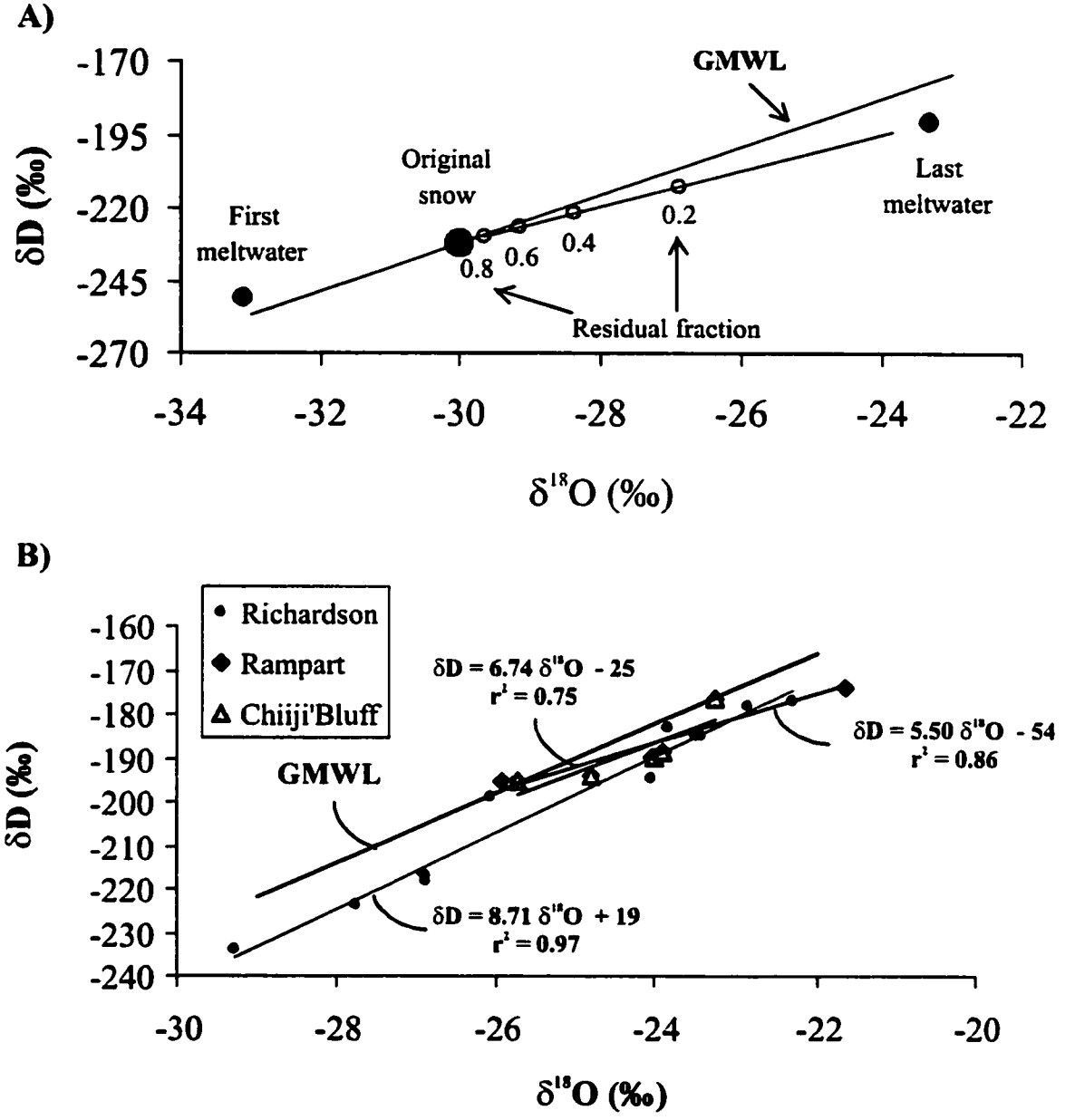

Figure 3.11: A) Simulation of the isotopic composition of water during melting of a snowpack (from Lauriol et al 1995). The original snow has a $\delta^{18}O$ equal to –30‰ and δD equal to –232‰. The gray line shows the evolution of $\delta^{18}O$ in the resulting snow meltwater, which after total melt has a $\delta^{18}O$ equal to –23‰. B) Co-isotope diagram of 3 ice wedges located in the western Canadian Arctic compared to the GMWL.

$\delta^{18}O$ variations from a core retrieved from a peat plateau

A 1.5 m long core was retrieved from the center of a peat plateau in a forested area (mostly Black Spruce) (67°30'N; 139°47'W). The stratigraphy consists of 0.7 m of peat, underlain by a gray silty-clay (gyttja). Radiocarbon dating indicates that the transition from the gyttja to peat began around 9950 ± 130 BP (UL–2387), with no evidence of cryoturbation. Peat accumulation was very slow, with only an increase of 0.35 m in peat thickness in the last 8200 years (8200 ± 90 BP; UL–2388). The interstitial water extracted above this depth reflects modern $\delta^{18}O$ since it is within the present active layer thickness, estimated to be ~ 0.30 m (Ovenden 1982).

Interstitial water extracted from the core are characterized by $\delta^{18}O$ values ranging from –23.5‰ to –21‰ (Figure 3.12 A), which is similar to the range of meteoric rainfall in the region. The mean $\delta^{18}O$ values recorded in the peat is –22.40‰ ± 0.4‰, while the mean $\delta^{18}O$ values from the gyttja is –22.01‰ ± 0.9‰. The $\delta^{18}O$ profile from 0.50 m to 1 m is characteristic of freezing from above and below. It may indicate the presence of a paleo-active layer at 8200 BP. On a δD–$\delta^{18}O$ diagram (Figure 3.12 B), the waters extracted below the paleo-active layer are clustered together and offset to the right with respect the waters extracted above it. The more enriched $\delta^{18}O$ values are located in the gyttja and attributed to the warmer climatic conditions of the early Holocene during the open water body phase (Mercier 2002).

The interstitial waters extracted above the paleo-active layer are aligned on a slope of 6.61 ($\delta D = 6.61\ \delta^{18}O - 26$; $r^2 = 0.95$), and may define a LMWL for the Old Crow – Bluefish Basins. This slope ($S = 6.61$) is less steep than the MWL defined for Inuvik ($S =$ 7.0; Vardy et al. 1998) but steeper than the MWL defined for Mayo ($S = 6.27$), indicating

that the vapour source traveled further inland and experienced a change in relative humidity before reaching the ground. This is also indicated by the lower deuterium excess for these waters (*d*-value = 4.6‰), compared with the deuterium excess for Inuvik (*d*-value = 13‰), suggesting greater secondary evaporation during rainfall.

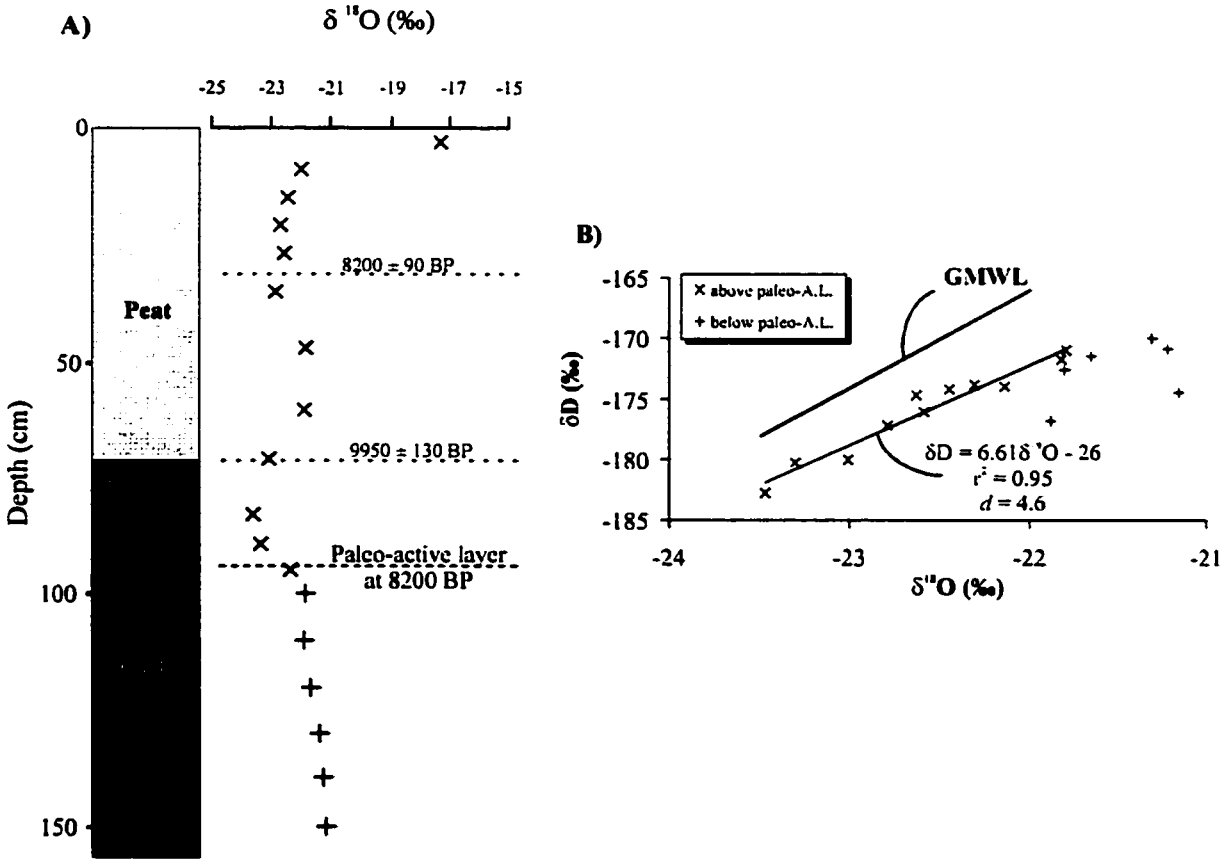

Figure 3.12: A) $\delta^{18}O$ profile of porewaters extracted from core BF-1. A ^{14}C date of 9950 BP was obtained at the contact between the peat and the gyttjia. B) δD– $\delta^{18}O$ diagram of porewaters extracted from BF-1 compared to the GMWL.

$\delta^{18}O$ signature of Pleistocene segregated ice

Lenticular and reticulate segregated ice, formed 2 m below the present ground surface within glaciolacustrine sediments, was sampled in an exposure along the Porcupine River in 1998. The glaciolacustrine (unit 5) sediments were deposited by glacial Lake Old Crow after 25,000 BP until 12,500 BP (Schweger 1989), by which time the lake had drained through the Rampart of the Porcupine to the west. Dyke (1996) indicated that permafrost was fully established in the Old Crow area by 10,000 BP. The water (ice) is characterized by a uniform $\delta^{18}O$ composition ranging from –24.7‰ to –24.4‰ (Table 3.3) and plots below the GMWL (Figure 3.13), indicating that the $\delta^{18}O$ signature of the segregated ice was altered by freezing or received an input from isotopically different water. The seasonal $\delta^{18}O$ signal found in precipitation is not recorded in the $\delta^{18}O$ composition of the segregated ice, which suggests that the segregated ice might represent paleo-waters from glacial lake Old Crow. Moreover, the $\delta^{18}O$ values are in the same range as glacial meltwater recorded in more southern regions. Remenda et al. (1994) found a uniform $\delta^{18}O$ value of –25‰ from Late Pleistocene clay deposits from glacial lake Agassiz, and from tills in southern Saskatchewan and in northern Ontario.

Paleo-climatic reconstructions suggest that the late Wisconsin climate was much colder and arid than present (Hughes et al. 1981). The only reliable data source that reflects the isotopic composition of precipitation during the Late Wisconsin comes from climatic records preserved in the Canadian Arctic ice cores (Paterson et al. 1977; Zdanowicz et al. 2002) more than 3000 km away. Precipitation during this time were highly depleted in $\delta^{18}O$ values (–35‰ to –30‰). The difference of 6–10‰ between the

segregated ice and the Wisconsin precipitation is too great to explain by fractionation alone, even if ambient precipitation would make this value slightly higher.

It can be assumed that the isotopic composition of the segregated ice should largely reflect the isotopic composition of the ice-dammed Lake Old Crow. The latter is mostly influenced by the isotopic composition of: (1) non-glacial water input from the Porcupine/Peel Rivers and (2) glacial runoff from the Laurentide ice sheet during its decay. The sedimentological record of deposition from Lake Old Crow suggests that it is the product of non-glacial processes dominated by inflow from unglaciated areas (Lemmen et al. 1994; Catto 1987). Dyke (1996) indicated that permafrost was fully established in the Old Crow region by 10,000 BP. The occurrence of permafrost served as an aquitard during the early Holocene warm interval, preventing mixing with isotopically enriched Holocene waters. Therefore, it can be assumed that the segregated ice is contemporaneous with the glaciolacustrine sediment of lake Old Crow.

The isotopic composition of non-glacial runoff from the paleo Porcupine and Pell Rivers have not been quantified. Figure 3.13 shows the isotopic distribution of the Wisconsinan precipitation recorded in the Barnes Ice Cap, the debris-rich ice formed in the Richardson Mountains, and that of the segregated ice. The three groups are separate and plot on distinct slopes. A freezing curve cannot be calculated for the segregated ice, owing to their high degree of clustering. However, it can be observed from figure 3.13 that the segregated ice falls along the freezing curve of the hypothesized segregated-intrusive ice derived from glacial meltwater in the Richardson Mountains. A steady enrichment in isotopes is observed in the direction of flow of the glacial meltwater (East to West). The most enriched group (Lake Old Crow segregated ice) is the most distal

from the maximum extension of the Laurentide ice sheet. Enrichment in the order of 3.5‰ in $\delta^{18}O$ is observed between the segregated ice and the segregated-intrusive ice in the Richardson Mountains (chapter 2). This enrichment is slightly greater than freezing conditions at equilibrium. A contribution from local precipitation would make the isotopic composition of glacial lake Old Crow slightly higher than that of glacial meltwater.

It can be hypothesized that the segregated ice found in the glacio-lacustrine sediment resulted from freezing of lake Old Crow waters (~ –27‰), which caused an isotopic enrichment in the order of 2–3‰ with respect to the water from which it is derived. The presence of an aquitard provided by the presence of permafrost suggests that for the most part, the water (ice) represents precipitation from the region, with additional input from glacial meltwater.

Table 3.3: $\delta^{18}O$ and δD values of segregated ice found within the glaciolacustrine sediment deposited by glacial lake Old Crow.

Sample no.	*$\delta^{18}O$ (‰)*	*δD (‰)*
970704 2	-24.5	-199
970704 3	-24.5	-200
970704 4	-24.7	-201
970704 5	-24.5	-200
970704 7	-24.5	-203
970704 8	-24.4	-199
970704 10	-24.6	-200
970704 14	-24.6	-202
970704 15	-24.5	-200
Mean	-24.5	-201
Std. Dev.	0.1	1

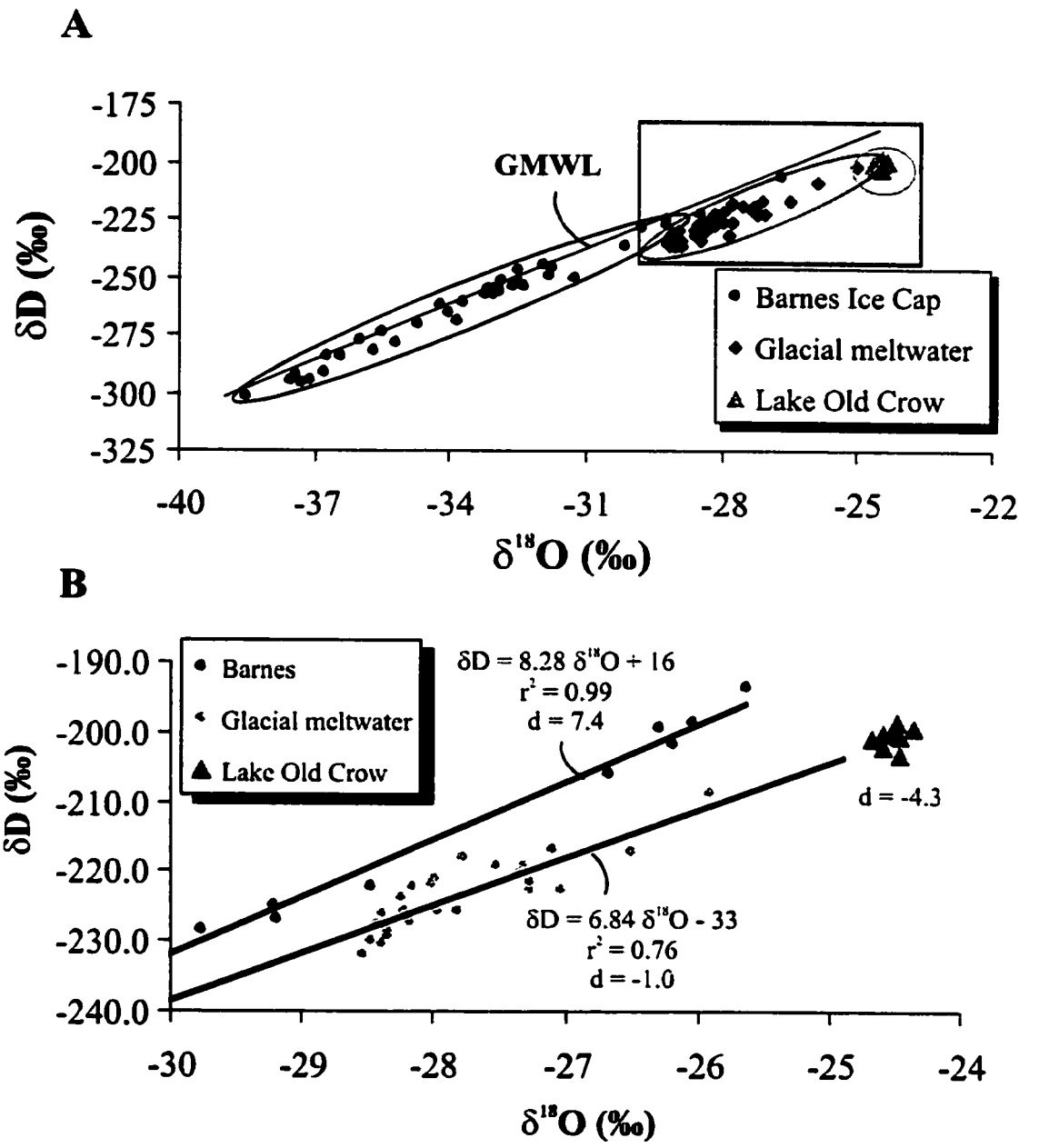

Figure 3.13: $\delta^{18}O$ - δD diagram showing the possible evolution of water from ice samples collected from the Barnes ice cap (Zdanowicz et al. 2002), glacial meltwater from the Laurentide ice sheet (this study), and segregated ice within the glaciolacustrine sediments of lake Old Crow (this study).

3.5 DISCUSSION

A summary of the $\delta^{18}O$ signature of meteoric, surface and subsurface ice in the Northern Yukon is presented in figure 3.14 A. The $^{18}O/^{16}O$ ratio is dependent upon a number of factors, such as surface air temperatures, history of the groundwater prior to freezing, and fractionation during freezing.

Changes in temperature and precipitation pattern are the basis for climate change. Given the good correlation between $\delta^{18}O$ and surface air temperature, climate change should be recorded in paleo-groundwater (ice). The climatic transition from Pleistocene glacial to Holocene interglacial conditions is recorded in the $\delta^{18}O$ values of ground ice. Pleistocene age ice (i.e. intrasedimental ice, buried glacier ice) is the most depleted in $\delta^{18}O$ (–35‰ to –27‰) indicating colder surface air temperatures at the time of formation. These ice types are associated either with a very cold paleo-groundwater source such as glacial meltwater (chapter 2) or might represent remnants of Wisconsinan glacier ice (Lorrain and Demeur 1985). Holocene age ice (i.e. ice wedge ice, active layer ice) have $\delta^{18}O$ values > –27‰ indicating a shift to warmer surface air temperature during the Holocene.

Figure 3.14 B shows the effect of freezing and evaporation on the various ice types in Northern Yukon. The extent of fractionation accompanying freezing is dependent on the freezing rate (Michel 1982). Slow freezing rates are accompanied by equilibrium isotopic fractionation, whereas when the freezing rate is rapid, little fractionation occurs. Isotopic fractionation should be observed during the formation of ground ice in Northern Yukon, since freezing rates are usually slower for a gradual temperature change.

The effect of evaporation follows a well-defined trend that is a function of relative humidity and temperature (Gonfiantini 1986) and is best observed on open surfaces. Open water bodies (thermokarst lakes) and active layer ice in the Bluefish Basin are enriched in the order of 5‰ to 11‰ with respect to the weighted mean $\delta^{18}O$ of precipitation (–24‰). Vardy et al. (1997) have shown that open peatlands in the Tuktoyaktuk Peninsula were enriched by as much as 9.5‰ as a result of low humidity conditions and Harris et al. (1992) have shown that active layer ice in a peat plateau also revealed signs of evaporation effect. Due to a relatively dry climate in the Bluefish Basin, evaporation plays an important role in the water balance of open surfaces and demonstrates how the residence time of groundwater in the supra-permafrost zone can effect the extent of evaporation. When the water table is close to the surface, there is little capacity to absorb additional water, therefore, run-off is rapid; however continuous thawing of the active layer increases surface storage capacity and decreases surface flow, thereby enhancing evaporation. This stresses the fact that on a small scale, stable isotopes are sensitive indicators to microclimatic and hydrological processes and must be analyzed with caution if paleoclimatic reconstructions are to be made.

The study of the isotopic composition of various ground ice formation in the Northern Yukon has allowed for a better understanding of the role that relative humidity plays prior to freezing and on the extent of fractionation that occurs during the freezing period on the isotopic composition of ground ice.

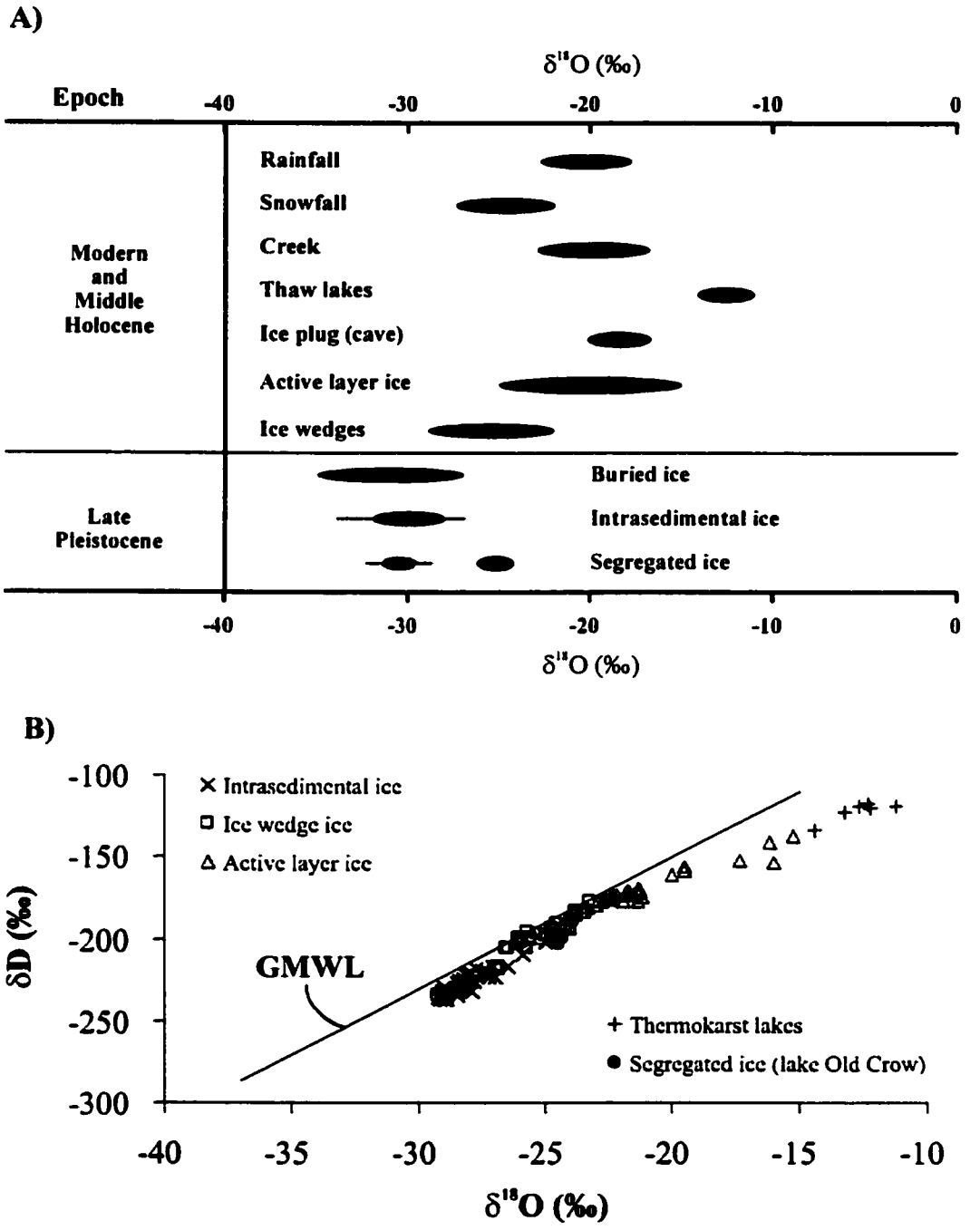

Figure 3.14: Synthesis of the range and kinetic effect on $\delta^{18}O$ and δD in meteoric, surface and subsurface ice in the western Canadian Arctic. The precipitation data is for Inuvik, NWT (Source: IAEA 1998), while the isotopic composition of the ice types is from various locations in the Northwestern Canada.

3.6 FUTURE RESEARCH

The study of the formation of ground ice bodies inferred from $\delta^{18}O$ and δD in the western Canadian Arctic has suggested a few possible avenues for future work.

First, other proxies, such as major ion concentration and noble gases concentrations should be analyzed in order to better understand the origin of groundwater.

Second, a systematic study of the relationship between glacial history, permafrost evolution and ground ice formation should be undertaken in order to better elucidate the origin of massive ground ice bodies in the western Canadian Arctic.

Hopefully, this thesis will encourage others to explore these avenues.

References

ACGR (Associated Committee on Geotechnical Research). 1988. Glossary of permafrost and related ground ice terms. Permafrost Subcommittee, National Research Council of Canada Technical Memorandum 142, 156p.

Astakhov, V.I. 1986. Geological conditions for the burial of Pleistocene glacier ice on the Yenisey. Polar Geography and Geology, 10: 286-295.

Beget, J. 1987. Low profile of the northwest Laurentide map sheets. Arctic and Alpine Research, 19: 81-87.

Boike, J. and Hubberten, H.W. 1998. Climatological and hydrological influences on stable hydrogen and oxygen isotopes of active layer waters, Levinson-Lessing lake area, Taymyr Peninsula. In; Proceedings, 7th International Permafrost Conference, Yellowknife, Canada p.65-70.

Bostock, H.S. 1948. Physiography of the Canadian Cordiller, with special reference to the area north of the fifty-fifth parallel. Geological Survey of Canada, Memoir 247, 106p.

Brown, R.J.E. 1978. Permafrost map of Canada. Plate 32 in Hydrological Atlas of Canada. Department of Fisheries and Environment. Ottawa, Canada.

Burn, C.R. 1997. Cryostratigraphy, paleogeography, and climate change during the early Holocene warm interval, western Arctic coast, Canada. Canadian Journal of Earth Sciences, 34: 912-925.

Burn, C.R. 2001. Permafrost. In; Occasional Papers in Earth Sciences No.2. Field guide to Quaternary research in central and western Yukon Territory. Eds. Froese, D.G., Duk-Rodkin, A. and Bond, J. August 2001. Whitehorse. p. 10-13.

Burns, B.M. 1974. The climate of the Mackenzie Valley. Environment Canada, Climatological Studies, Volume 2, No.24.

Canadian National Committee for the International Hydrological Decade. 1978. Hydrological Atlas of Canada. Fisheries and Environment Canada, Ottawa, 150p.

Catto, N.R. 1986. Quaternary Sedimentology and Stratigraphy, Peel Plateau and Richardson Mountains, Yukon and N.W.T. Unpublished PhD Thesis. University of Edmonton. 723p.

Catto, N.R. 1987. Lacustrine sedimentation in a proglacial environment, Caribou River Valley, Yukon, Canada. Boreas, 16: 197-206.

Cheng, G. 1983. The mechanism of repeated-segregation for the formation of thick layered ground ice. Cold Regions Science and Technology, 8: 57-66.

Clark, I.D. and Fritz, P. 1997. Environmental Isotopes in Hydrogeology. Lewis Publisher. U.S.A. 328p.

Craig, H. 1961. Isotopic variations in meteoric waters. Science, 133: 1702-1703.

Dallimore, S.R. and Wolfe, S.A. 1988. Massive ground ice associated with glaciofluvial sediments, Richards Island, N.W.T., Canada. In: Permafrost, 5th International Conference on Permafrost. Tapir, Trondheim, Norway, p. 132-137.

Dansgaard, W. 1964. Stable isotopes in precipitation. Tellus, XVI(4): 436-468.

Duk-Rodkin, A. and Hughes, O.L. 1992. Surficial geology, Fort McPherson-Bell River, Yukon-Northwest Territories; Geological Survey of Canada, Map 1745A, scale 1:250,000.

Duk-Rodkin, A. and Hughes, O.L. 1995. Quaternary geology of the northeastern part of the central Mackenzie Valley corridor, district of Mackenzie, Northwest Territories. Geological Survey of Canada, Bulletin 458, 45p.

Duk-Rodkin, A. and Froese, D.G. 2001. Yukon Glacial History. In; Occasional Papers in Earth Sciences No.2. Field guide to Quaternary research in central and western Yukon Territory. Eds. Froese, D.G., Duk-Rodkin, A. and Bond, J. August 2001. Whitehorse. p. 14-16.

Dyke, A.S. 1996. Preliminary paleogeographic maps of glaciated North America. Geological Survey of Canada. Open Files 3296, 6pp.

Environment Canada. 2001. Historical Canadian Climate Database: Monthly Rehabilitated Precipitation and Homogenized Temperature Datasets for Inuvik and Old Crow. Climate Monitoring and Data Interpretation Division for the Climate Research Branch, Meteorological Service of Canada. URL: cccma.bc.ec.gc.ca/hccd/

French, H.M. 1996. The Periglacial Environment. Second edition, Longman. Harlow. 341p.

French, H.M. and Pollard, W.H. 1986. Ground-ice investigations, Klondike District, Yukon Territory. Canadian Journal of Earth Sciences, 23: 550-560.

French, H.M. and Harry, D.G. 1990. Observation on buried glacier ice and massive segregated ice, Western Arctic Coast, Canada. Permafrost and Periglacial Processes, 1: 31-43.

Fujino, K., Sato, S., Matsuda, K., Sada, G., Shimizu, O. and Kato, K. 1988. Characteristics of the massive ground ice body in the western Canadian Arctic. In; Proceedings, 5th International Conference on Permafrost, August 1988, Trondheim, Norway, p.143-147.

Gonfiantini, R. 1986. Environmental isotopes in lake studies. In; Fritz, P. and Fontes J.C. (eds) Handbook of environmental isotope geochemistry, Vol. 2, The Terrestrial Environment., B. Elsevier, Amsterdam, p.113-168.

Harris, S.A., Schmidt, I.H. and Krouse, H.R. 1992. Hydrogen and oxygen isotopes and the origin of the ice in peat plateaus. Permafrost and Periglacial Processes, 3: 19-27.

Harry, D.G., French, H.M. and Pollard, W.H. 1988. Massive ground ice and ice-cored terrain near Sabine Point, Yukon Coastal Plain. Canadian Journal of Earth Sciences, 25: 1846-1856.

Hubbard, B. and Sharp, M. 1997. Basal ice formation and deformation: a review. Progress in Physical Geography, X: 529-558.

Hughes, O.L., Harington, C.R., Janssens, J., Matthews, J.V., Morlan, R.E., Rutter, N.W. and Schweger, C.E. 1981. Upper Pleistocene stratigraphy, paleoecology, and archeology of the northern Yukon interior, eastern Beringia, 1: Bonnet Plume Basin. Arctic, 34: 329-365.

IAEA/WMO. 1998. Global network for isotope in precipitation. The GNIP database, Release 3, October 1999. URL: http://www.iaia.org/programs/ri/gnip/gnipmain.htm.

Jouzel, J. and Souchez, R.A. 1982. Melting-Refreezing at the glacier sole and isotopic composition of the ice. Journal of Glaciology, 28(98): 35-41.

Judge, A. 1973. The prediction of permafrost thickness. Canadian Geotechnical Journal, 10: 1-11.

Kaplanskaya, F.A. and Tarnogradski, V.D. 1986. Remnants of the Pleistocene ice sheets in the permafrost zone as an object for paleoglaciological research. Polar Geography and Geology, 10: 257-266.

Kasper, J.N. and Allard, M. 2001. Late-Holocene climatic changes as detected by the growth and decay of ice wedges on the southern shore of Hudson Strait, northern Québec, Canada. The Holocene, 11,5: 563-577.

Karpov, Y.E. 1986. Morphology of a tabular body of ground ice and the dynamics of the development of the Ledyanaya Gora exposure. Polar Geography and Geology, 10: 267-272.

Klassen, R.A. and Shilts, W.W. 1987. Bylot Island, Eastern Canadian Arctic. XII Inqua Congress Field Excursion A-1 Guidebook, 54p.

Knight, P.G. 1997. The basal ice layer of glaciers and ice sheets. Quaternary Sciences Reviews, 16: 975-993.

Lamirande, I., Lauriol, B., Lalonde, A.E. and Clark, I.D. 1999. La production de limon sur des terrasses de cryoplanation dans les monts Richardson, Canada. Canadian Journal of Earth Sciences, 36: 1645-1654.

Langway Jr., C.C. 1958. Ice fabrics and the universal stage. U.S. army snow ice and permafrost research establishment. Technical Report 62, 16p.

Lauriol, B. and Clark, I.D. 1993. An approach to determine the origin and age of massive ice blockages in two arctic caves. Permafrost and Periglacial Processes, 4: 77-85.

Lauriol, B., Duchesne, C. and Clark, I.D. 1995. Systématique du remplissage en eau des fentes de gel: les resultants d'une étude oxygène-18 et deuterium. Permafrost and Periglacial Processes, 6: 47-55.

Lauriol, B., Bjornson, J., Cinq-Mars, J., Clark, I.D. and Lacelle, D. 2001. Geomorphological responses to climate change in the Canadian North during the Holocene: importance of their recognition. Occasional Papers in Earth Sciences No.1, Canadian Quaternary Association Meetings, 2001, Whitehorse, Yukon, 46-47.

Lauriol, B., Duguay, C.R. and Riel, A. 2002. Response of the Porcupine and Old Crow rivers in Northern Yukon to Holocene climate change. The Holocene, 12,5: 27-34.

Lemmen, D.S., Duk-Rodkin, A. and Bednarski, J.M. 1994. Late glacial drainage systems along the northwestern margin of the Laurentide ice sheet. Quaternary Science Reviews, 13: 805-828.

Lewkowicz, A.G. 1994. Ice wedge rejuvenation, Fosheim Peninsula, Ellesmere Island, Canada. Permafrost and Periglacial Processes, 5: 251-268.

Lorrain, R.D. and Demeur, P. 1985. Isotopic evidence for relic Pleistocene glacier ice on Victoria Island, Canadian Arctic Archipelago. Arctic and Alpine Research, 17: 89-98.

Mackay, J.R. 1966. Segregated epigenetic ice and slumps in permafrost, Mackenzie delta area, N.W.T. Geographical Bulletin, 8: 59-80.

Mackay, J.R. 1971. The origin of massive icy beds in permafrost, Western Arctic, Canada. Science, 8: 397-422.

Mackay, J.R. 1972. The world of underground ice. Annals of the Association of American Geographers, 62: 1-22.

Mackay, J.R. 1983. Oxygen isotope variations in permafrost, Tuktoyaktuk Peninsula area, Northwest Territories. Current Research, Part B, Geological Survey of Canada, Paper 83-1B: 67-74.

Mackay, J.R. 1986. The first 7 years (1978-1985) of ice wedge growth, Illisarvik experimental drained lake site, western Arctic coast. Canadian Journal of Earth Sciences, 23: 1782-1795.

Mackay, J.R. 1989. Massive ice: Some field criteria for the identification of ice types. Current Research, Part G, Geological Survey of Canada, Paper 89-1G: 5-11.

Mackay, J.R. 1990a. Seasonal growth bands in pingo ice. Canadian Journal of Earth Sciences, 27: 1115-1125.

Mackay, J.R. 1990b. Some observations on the growth and deformation of epigenetic, syngenetic and anti-syngenetic ice wedges. Permafrost and Periglacial Processes, 1: 15-29.

Mackay, J.R. 2000. Thermally induced movements in ice-wedge polygons, western Arctic coast: A long-term study. Géographie Physique et Quaternaire, 54: 41-68.

Mackay, J.R. and Dallimore, S.R. 1992. Massive ice of the Tuktoyaktuk area, western Arctic coast, Canada. Canadian Journal of Earth Sciences, 29: 1235-1249.

Mercier, G. 2002. Macrofossils analysis from peatlands, Bluefish Basin, Yukon Territory. B.A. Thesis. University of Ottawa. 78p.

Michel, F.A. 1982. Isotope investigations of permafrost waters in northern Canada. Unpublished PhD Thesis, University of Waterloo. 424p.

Michel, F.A. 1990. Isotopic composition of ice wedges in northwestern Canada. Nordicana, 54: 5-9.

Michel, F.A. and Fritz, P. 1982. Siginificance of isotope variations in permafrost waters at Illisarvik, N.W.T. Proceedings, 4th Canadian Permafrost Conference, Calgary, Alberta, p.173-181.

Moser, H. and Stichler, W. 1980. Environmental isotopes in ice and snow. In Fritz, P. and Fontes, J.C. (eds), Handbook of Environmental Isotope Geochemistry. Vol. 1: The Terrestrial Environment. Elsevier, Amsterdam, p. 141-178.

Murton, J.B. 1993. Thermokarst sedimentology of the Tuktoyaktuk Coastlands, NWT. Unpublished PhD Thesis. University of Ottawa. 193p.

Murton, J.B. and French, H.M. 1994. Cryostructures in permafrost, Tuktoyaktuk coastlands, western Arctic Canada. Canadian Journal of Earth Sciences, 31: 737-747.

Nikolayev, V.I. and Mikhalev, D.V. 1995. An oxygen-isotope paleothermometer from ice in Siberian permafrost. Quaternary Research, 43: 12-21.

Norris, D.K. 1981. Geology of Old Crow Yukon Territory, 1:250 000, Ottawa: Geological Survey of Canada, map 1518A.

Norris, D.K. 1984. Geology of the Northern Yukon and Norhtwest district of Mackenzie, 1:500,000, Ottawa: Geological Survey of Canada, map 1581A.

O'Leary, M.H. 1988. Carbon isotopes in photosynthesis. Bioscience, 38: 328.

O'Neil, J.R. 1968. Hydrogen and oxygen isotope fractionation between ice and water. Journal of Physical Chemistry, 72: 3683-3684.

Ovenden, L. 1982. Vegetation history of a polygonal peatland, northern Yukon. Boreas, 11: 209.224.

Parks Canada. 2000. Vuntut National Park. Resource description and analysis.

Paterson, W.S.B., Koerner, R.M., Fisher, D., Johnson, S.J., Clausen, H.B., Dansgaard, W., Bucher, P. and Oeschger, H. 1977. An oxygen-isotope climatic record from the Devon Island ice cap, Arctic Canada. Nature, 266: 588-611.

Pollard, W.H. and French, H.M. 1980. A first approximation of the volume of ground ice, Richards Island, Pleistocene Mackenzie Delta, Northwest Territories, Canada. Canadian Geotechnical Journal, 17: 509-516.

Pollard, W.H. and French, H.M. 1984. The groundwater hydraulics of seasonal frost mounds, Northern Yukon. Canadian Journal of Earth Sciences, 21: 1073-1081.

Pollard, W.H. and French, H.M. 1985. The internal structure and ice crystallography of seasonal frost mounds. Journal of Glaciology, 31: 157-162.

Pollard, W.H. and Dallimore, S.R. 1988. Petrographic characteristics of massive ground ice, Yukon Coastal Plain, Canada. In; Proceedings, 5th International Conference on Permafrost, August 1988, Trondheim, Norway, p.224-229.

Rampton, V.N. 1982. Quaternary Geology of the Yukon Coastal Plain, Canada. Geological Survey of Canada, Bulletin 317, 42p.

Rampton, V.N. 1988a. Quaternary Geology of the Tuktoyaktuk Coastlands, Northwest Territories. Geological Survey of Canada, Memoir 423, 98p.

Rampton, V.N. 1988b. Origin of massive ground ice on Tuktoyaktuk peninsula, Northwest Territories, Canada : A review of stratigraphic and geomorphic evidence. In; Proceedings, 5th International Conference on Permafrost, August 1988, Trondheim, Norway, p.850-855.

Rampton, V.N. 2001. Major en moraines of Younger Dryas age on Wollaston Peninsula, Victoria Island, Canadian Arctic: implications for paleoclimate and for formation of hummocky moraine: Discussion. Canadian Journal of Earth Sciences, 38: 1003-1006.

Remenda, V.H., Cherry, J.A. and Edwards, T.W.D. 1994. Isotopic composition of old ground water from Lake Agassiz: Implications for Late Pleistocene climate. Science, 266: 1975-1978.

Ritchie, J.C. 1984. The past and present vegetation of the Far Northwest of Canada. University of Toronto Press, Toronto, Canada, 284p.

Schroeder, J. 1977. Les formes des glaces des grottes de la Nahanni, Territoires du Nord-Ouest, Canada. Canadian Journal of Earth Sciences, 14: 21-24.

Schweger, C.E. 1989. The Old Crow and Bluefish Basins, Northern Yukon: Development of the Quaternary history. In; Late Cenozoic history of the interior basins of Alaska and Yukon. Carter, L.D. and Hamilton, T.D. (eds), USGS Circular 1026 p.30-33.

Souchez, R.A. and Jouzel, J. 1984. On the isotopic composition in δD and $\delta^{18}O$ of water and ice during freezing. Journal of Glaciology, 30: 369-372.

Souchez, R.A. and de Grotte, J.M. 1985. δD - $\delta^{18}O$ relationships in ice formed by subglacial freezing: paleoclimatic implications. Journal of Glaciology, 30: 369-372.

Souchez, R.A., Lorrain, R., Tison, J.L. and Jouzel, J. 1988. Co-isotopic signature of two mechanisms of basal-ice formation in arctic outlet glaciers. Annals of Glaciology, 10: 163-166.

Souchez, R.A. and Lorrain, R.D. 1991. Ice composition and glacier dynamics. Springer, Berlin, 270p.

Sollid, J.L. and and Sorbel, L. 1988. Influence of temperature conditions in formation of end moraines in Fennoscandian and Svalbard. Boreas, 17: 553-558.

St-Onge, D.A. and McMartin, I. 1995. Quaternary Geology of the Inman River area, Northwest Territoies. Geological Survey of Canada, Bulletin 446, 59p.

Troutet, Y. 2002. CO_2 content and isotopes in ground ice: Implications for the origin of tabular ice beds in Canada's western Arctic. B.Sc. Thesis. University of Ottawa.

Vardy, S.R., Warner, B.G. and Aravena, R. 1998. Holocene climate and the development of a subarctic peatland near Inuvik, Northwest Territories, Canada. Climatic Change, 40: 285-313.

Wahl, H.E., Fraser, D.B., Harvey, R.C. and Maxwell, J.B. 1987. Climate of Yukon. Environment Canada, Atmospheric Environment Service, Toronto, 323p.

Washburn, A.L. 1980. Geocryology: a survey of periglacial processes and environments. Wiley, New York, 406p.

Worsley, P. 1999. Context of relic Wisconsinan glacial ice at Angus Lake, SW Banks Island, Western Canadian Arctic and stratigraphic implications. Boreas,, 28: 543-550.

Zdanowicz, C.M., Michel, F.A. and Shilts, W.W. 1996. Basal debris entrainment and transport in glaciers of southwestern Bylot Island, Canadian Arctic. Annals of Glaciology, 22: 107-113.

Zdanowicz, C.M., Fisher, D., Clark, I.D. and Lacelle, D. 2002. An ice-marginal $\delta^{18}O$ record from Barnes Ice Cap, Baffin Island, Canada. Annals of Glaciology, 35.